Journal of Sound and Vibration 589 (2024) 118538

Contents lists available at ScienceDirect

Journal of Sound and Vibration

journal homepage: www.elsevier.com/locate/jsvi

Equivalent damping ratio oriented investigation on tuned negative stiffness inerter damper for seismic application

Hui He [a,c], Linfei Hao [b,*], Yun Zhou [c], Zicong Lin [b], Yue Xiang [b], Yafeng Li [b,c]

[a] Hunan Institute of Technology, Hengyang 421002, PR China
[b] Guangdong Provincial Key Laboratory of Earthquake Engineering and Applied Technology, Guangzhou Univesity, Guangzhou 510006, PR China
[c] College of Civil Engineering, Hunan University, Changsha 410082, PR China

ARTICLE INFO

Keywords:
Tuned negative stiffness inerter dampers
Inerter-based dampers
Negative stiffness elements
Tuned inerter dampers
Equivalent damping ratio

ABSTRACT

Additional equivalent damping ratio (EDR) plays a crucial role in the performance evaluation and design methodology of conventional passive dampers. The inclusion of inerter elements has been extensively demonstrated to significantly enhance the control efficiency of these passive dampers. Recently, negative stiffness (NS) elements have been found potential to enhance the control performance of inerter-based dampers (IBDs). However, little research has investigated the enhancement effect of NS elements on the additional EDR of IBDs. Meanwhile, the existing design methodology for IBDs is response-based, posing challenges in ensuring optimal control efficiency and fully utilizing the essential features of inerter and NS elements. In this study, the tuned negative stiffness inerter damper (TNSID), which integrates the NS element into one of the classical IBDs, namely the tuned inerter damper (TID), is investigated in terms of EDR for seismic application. This study makes two primary contributions. Firstly, it proposes an optimization design methodology aimed at achieving optimal control performance and efficiency of the TNSID simultaneously. Secondly, it unveils the enhancement law for the control performance and efficiency of TNSID. To do this, the analytical formulas for additional EDR and EDR enhancement (EDRE) factors are established as indicators of control performance and efficiency, respectively. Closed-form expressions are derived to optimize the TNSID design parameters. The comparative studies are conducted on both single and multi-degree-of-freedom primary structures, utilizing closed-form expressions, frequency transfer functions, and time history analysis. Results demonstrate that the incorporation of the NS element and the proposed optimization design methodology can further enhance both the control performance and efficiency of TNSID, surpassing those achieved by TID and classical fixed-point optimization theory.

1. Introduction

Structural vibration control plays a very important role in the design and retrofitting of civil structures to avoid damage from undesired vibration caused by external excitations [1–3]. Passive vibration control devices (passive dampers) have been widely used in structural vibration control [4–8], because of the advantages of independence from external energy, high reliability, and simple maintenance. Extensive research has been carried out on various devices to achieve a reduction in structural response through different energy dissipation mechanisms [9–13]. A common concern in these studies is to improve the control efficiency of the devices, i.e., how

* Corresponding author.
E-mail address: haolf@gzhu.edu.cn (L. Hao).

https://doi.org/10.1016/j.jsv.2024.118538
Received 14 November 2023; Received in revised form 1 May 2024; Accepted 24 May 2024
Available online 25 May 2024

to achieve the highest possible control performance with a smaller number of dampers or material consumption [14–17].

The inerter is a highly promising inertia element in improving the efficiency of structural vibration control. Its inertial force is based on the relative acceleration between the endpoints. A variety of mechanisms have been utilized for the implementation of inerters, including the utilization of a ball screw [18,19], rack and pinion systems [20], liquid pumps [21,22], and magnetorheology technology [23]. These mechanisms possess the capability to generate substantial inertial force and equivalent inertia mass despite their relatively small physical mass. The utilization of inerter elements for structural vibration control through the tuning function can enhance the control efficiency by exploiting the mass amplification effect.

Inerter-based dampers (IBDs) could be constituted by combining the inerter elements with the components of conventional dampers. Saito et al. [24] investigated the control performance of IBD by connecting parallel inerter and dashpot elements in series with a spring element to form a tuned viscous mass damper (TVMD). Ikago et al. [19] developed a TVMD device utilizing the ball screw-flywheel mechanism and the concept of a rotary viscous damper, which was subsequently validated through rigorous shaking table tests. Lazar et al. [25] proposed a tuned inerter damper (TID) by connecting the inerter element in series with parallel spring and dashpot elements. Marian et al. [26] added an inerter element between the tuned mass damper (TMD) and the structure or foundation to propose a tuned mass damper inerter (TMDI) system. Nakamura et al. [27] developed an electromagnetic inertia mass damper (EIMD), which consists of a ball screw-flywheel mechanism and a generator to produce an inertial force and a variable damping force, respectively. In these IBDs, the inerter elements amplify the deformation of the dashpot elements, thereby creating an energy dissipation amplification effect. This effect leads to an enhancement in vibration control efficiency.

Negative stiffness (NS) elements were initially introduced in the field of seismic resistance by Molyneaux [28] and Platus [29]. Unlike ordinary positive stiffness elements, the deformations of NS elements tend to increase when subjected to a force. Carrella et al. [30] developed a simple NS system containing one vertical spring and two inclined springs connected in parallel. Similar NS elements utilizing spring mechanisms were also presented in [31,32]. Shi and Zhu [33] introduced a magnetic NS system, which consists of several permanent magnets arranged within an electro-conductive pipe. The NS systems based on electromagnetic mechanisms could also be found in [34,35]. Furthermore, numerous studies have investigated the response mitigation performance when NS elements are combined with commonly used dampers such as viscous dampers (VD) [36–38], viscoelastic dampers (VED) [39], and TMD [40].

Recently, to further improve the vibration control performance of IBDs, the IBDs containing NS elements (NS-IBD) have received attention. Zhao et al. [41] proposed an NS inerter system (NSIS) that combines inerter and dashpot elements with an NS spring in parallel, and they are connected in series with a spring element. The analysis results demonstrated that significant energy dissipation efficiency and better control performance could be achieved across a wider frequency range. Ye et al. [42] proposed a TID_NSD comprising an NS element and a TID in parallel. The numerical analysis indicated that the optimized TID_NSD was more effective than the bare TID in controlling the structural displacement and acceleration responses. Barredo et al. [43] introduced the NS-NIDVA, a novel dynamic vibration absorber, by combining an NS element in parallel with a TID and connecting them in series with a TMD. The analysis results show that additional inerter and NS elements not only reduce the physical mass requirement of the dynamic vibration absorber but also enhance its control effectiveness. Wang et al. [44] developed a novel tuned inerter NS damper (TINSD) based on a ball screw mechanism and a magnetic-force-induced NS element. The comparison results demonstrate that TINSD is more efficient in reducing structural response than TID and TVMD. These studies suggest that incorporating NS elements could further enhance the efficiency of IBDs in controlling structural vibrations.

How to optimize the design parameters of the IBDs is another key issue to achieve efficient control. Numerous researches have been carried out on the optimal design methodology for different types of IBDs, among which the first class of representative methods are based on the H_∞ criterion. For single-degree-of-freedom (SDOF) structures, based on the H_∞ criterion, the optimal frequency and damping ratio of the supplemental TVMD were obtained by using the fixed-point strategy [45,46]. Jia et al. [47] applied TVMD at the extending arms to control the seismic response of frame-core wall structures and optimized the TVMD using the fixed-point strategy. Islam and Jangid [48] determined the optimal frequency and damping ratios of TID based on the fixed-point strategy considering the undamped SDOF primary structure. For the damped primary structure, the optimal parameters of TID were firstly obtained by numerical seeking, and then their closed-form expressions were given by fitting. Marian [49] also derived closed-form expressions for the optimal parameters of a TMDI added on an undamped primary structure based on the fixed-point strategy.

Another significant category of optimization methodology is based on the H_2 criterion, which utilizes structural mean square responses. Marian and Giaralis [50] employed the mean square displacement response of the primary structure as the objective to numerically optimize the TMDI utilizing the "min-max" constraint optimization algorithm. Sun et al. [51] compared the performance of ordinary isolated structures with that of isolated structures incorporating an inerter damper (ID) and the tuned inerter damper (TID). The study provides closed-form solutions for optimizing the design parameters of the dampers using the H_2 criterion. Chen and Tan [52] derived closed-form expressions for the optimal design parameters of a TVMD-linear structure system under white noise excitation, based on the H_2 criterion. The optimal damping and frequency ratios of TMDI under stationary and filtered white noise excitations were determined by Jangid [53] using a numerical searching technique. The structural vibration control problem was investigated by Djerouni et al. [54], focusing on the utilization of the double mass tuned damper inerter (DMTDI). They conducted an optimization process using a genetic algorithm, to minimize the H_2 norm of the roof displacement.

As for the NS-IBDs, the optimization methodology employing H_∞ and H_2 criteria has also been investigated. Ye et al. [42] determined the optimal frequency ratio, damping ratio, and NS of the TID_NSD by utilizing the H_∞ criterion. Wang et al. [44] derived closed-form expressions for the optimal design parameters of TINSD via the H_∞ criterion based on the SDOF primary structure. Islam et al. [55] and Li et al. [56] employed optimization approaches based on the H_∞ criterion to investigate IBDs involving NS elements. Moreover, Islam and Jangid [57] investigated H_2 optimal control of negative stiffness and inerter-based dampers as supplemental dampers to a damped SDOF system. The seismic response control performance of NS-IBDs for liquid storage tanks has also been

investigated [58]. Chowdhury et al. [59] developed negative stiffness inerter passive dampers such as negative stiffness inerter-based base isolators (NSIBI), negative stiffness base isolators (NSBI), negative stiffness inerter-based tuned mass dampers (NSITMD), and negative stiffness tuned mass dampers (NSTMD). The authors also proposed the corresponding optimization methodology based on H_2 and H_∞ criteria for these novel passive vibration dampers. Tai et al. [60] derived the analytical solution for the optimal design parameters of TINSD based on H_2 and H_∞ criteria. Wang et al. [61] proposed the analytical expressions for the optimal design parameters of two novel dynamic vibration absorbers, namely N-TID and N-TVMD, which incorporate inerter and negative stiffness. Su et al. [62] proposed an optimal design methodology for the NS-IBDs to balance static amplification and dynamic reduction effects. To balance the control performance and design cost, Gao et al. [63] proposed a demand-oriented optimum design methodology of the TNSID for the base-isolated structures. Kiran et al. [64] also provided fitting expressions for optimal design parameters of TINSD for isolated structures.

The fixed-point strategy based on H_∞ criteria is widely employed in optimization methodologies due to its ability to provide concise closed-form expressions for optimal parameters, rendering it particularly advantageous for engineering design, especially in the estimation of design parameters during the preliminary design phase. The optimization methodologies based on the structural mean square responses (e.g., H_2 criteria) can also provide closed-form expressions for the optimal parameters, while others necessitate numerical procedures and offer greater flexibility in considering diverse optimization objectives, thereby providing enhanced accuracy. It is noted that the H_∞ and H_2 criteria-based optimization methodologies both utilize the structural response level as an indicator of control performance. However, the structural response level alone fails to adequately capture the control efficiency of NS-IBDs, i.e., the extent to which inerter and NS elements can enhance control performance compared to conventional passive dampers like VD. The enhancement of control performance, as previously indicated, is a crucial attribute of both the inerter and NS elements, thus necessitating its consideration in the optimal design process. Meanwhile, the additional equivalent damping ratio (EDR) provided by the damper to the primary structure is widely recognized as a significant performance index in various design codes and guidelines [65-68], making it familiar to engineers. From a practical point of view, the integration of existing design methods for IBDs and NS-IBD with the design concepts based on additional EDR becomes intricate due to their predominantly structural response-oriented nature.

In response to the aforementioned issues, the evaluation of additional EDR provided by IBDs and the development of corresponding optimization methods for maximizing control performance enhancement have garnered attention in existing studies. Zhang et al. [69] developed an analytical relationship between the vibration control performance of TVMDs and their damping enhancement effect. Moreover, a numerical optimization scheme for the IBD parameters was formulated, with the objectives of structural response reduction factor and damping enhancement level. Pan et al. [70] derived an analytical expression for the additional EDR provided by TVMD considering the stochastic response of SDOF structures with TVMD and gave closed-form expressions to optimize the design parameters for maximum damping enhancement. Hao et al. [71] developed expressions for the additional EDR and its enhancement factor for SDOF and MDOF structures equipped with TID. The TID locations were considered, and closed-form expressions for the optimal parameters based on the control performance and control efficiency were given. Li et al. [72] presented an optimal design process for a novel tuned inerter eddy current damper (TIECD) based on the additional EDR and its enhancement effect.

However, the additional EDR of NS-IBDs and their control performance enhancement have not been sufficiently investigated. As stated above, the evaluation of the additional EDR of NS-IBDs facilitates a comparative analysis of control performance with conventional passive dampers based on identical indices, enabling optimal design based on a general concept. The incorporation of NS elements is crucial in IBDs as it significantly enhances control efficiency, serving as one of the primary objectives. Therefore, the optimization of NS-IBDs to maximize their enhancement effect, considering the additional improvement brought by NS on the control efficiency of IBDs through EDR, can facilitate the comprehensive application of the inerter and NS elements.

This study focuses on one typical type of NS-IBDs, namely TNSID, which comprises the TID attached to NS elements. The objective of this study is to investigate the structural vibration control performance and control efficiency of TNSID from the perspective of additional EDR. The organization of this study is as follows. Section 2 presents evaluation formulas for additional EDR and equivalent damping ratio enhancement (EDRE) factor of TNSID, which serve as indicators of vibration control performance and control efficiency,

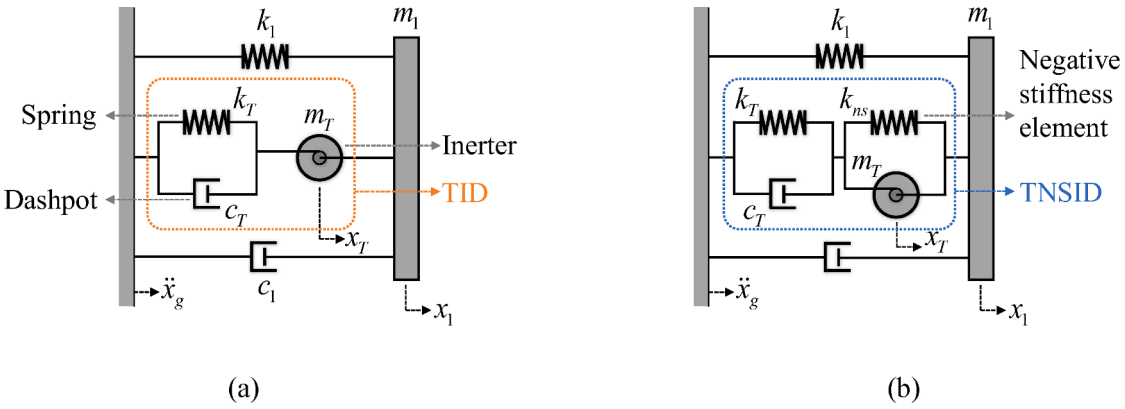

Fig. 1. Schematic for an SDOF primary structure equipped with (a) TID and (b) TNSID.

respectively. Section 3 develops closed-form expressions for the optimal design parameter of the TNSID, utilizing the two indicators as optimization objectives. By considering the SDOF and MDOF primary structures coupled with TNSIDs, Section 4 verifies the enhancement effect of additional NS elements on TID control efficiency, as well as confirms the validity of the proposed optimization methodology.

2. Theoretical analysis

In this section, the theoretical model for the SDOF primary structure coupled with a TNSID is provided. The formulas for the additional EDR of TNSID are derived based on the assumption that the seismic excitations are ideal white noise processes. The EDRE factor is introduced to demonstrate the improved control performance of TNSID resulting from the incorporation of inerter and NS elements.

2.1. Theoretical model of SDOF structure coupled with TNSID

To improve the control performance of an IBD like TID (Fig. 1(a)), TNSID is explored by combining the NS, inerter, spring, and dashpot elements, as shown in Fig. 1(b). Let m_1, k_1, and c_1 denote the mass, stiffness, and damping coefficient of the primary structure, respectively; m_T, k_T, and c_T represent the TNSID inertia mass, stiffness, and damping coefficient, respectively; k_{ns} is the stiffness coefficient of the NS element; x_T denotes the deformation of the inerter and NS elements; x_1 is the displacement of the primary structure relative to the ground. The governing motion equations of the structure-TNSID system subjected to the seismic ground motion $\ddot{x}_g$ could be written as:

$$\begin{bmatrix} m_1 & 0 \\ 0 & m_T \end{bmatrix} \begin{Bmatrix} \ddot{x}_1 \\ \ddot{x}_T \end{Bmatrix} + \begin{bmatrix} c_1 + c_T & -c_T \\ -c_T & c_T \end{bmatrix} \begin{Bmatrix} \dot{x}_1 \\ \dot{x}_T \end{Bmatrix} + \begin{bmatrix} k_1 + k_T & -k_T \\ -k_T & k_T + k_{ns} \end{bmatrix} \begin{Bmatrix} x_1 \\ x_T \end{Bmatrix} = -\begin{Bmatrix} m_1 \\ 0 \end{Bmatrix} \ddot{x}_g. \tag{1}$$

By defining the system parameters listed in Table 1, Eq. (1) could be rewritten as:

$$\begin{bmatrix} 1 & 0 \\ 0 & \mu \end{bmatrix} \begin{Bmatrix} \ddot{x}_1 \\ \ddot{x}_T \end{Bmatrix} + \begin{bmatrix} 2(\zeta_1 + \zeta_T)\omega_1 & -2\zeta_T\omega_1 \\ -2\zeta_T\omega_1 & 2\zeta_T\omega_1 \end{bmatrix} \begin{Bmatrix} \dot{x}_1 \\ \dot{x}_T \end{Bmatrix} + \begin{bmatrix} (1+\mu\gamma^2)\omega_1^2 & -\mu\gamma^2\omega_1^2 \\ -\mu\gamma^2\omega_1^2 & (1+\beta)\mu\gamma^2\omega_1^2 \end{bmatrix} \begin{Bmatrix} x_1 \\ x_T \end{Bmatrix} = -\begin{Bmatrix} 1 \\ 0 \end{Bmatrix} \ddot{x}_g. \tag{2}$$

Assuming that the frequency of the seismic ground motion is ω, the displacement frequency transfer function of the primary structure could be obtained as:

$$H_1^{\mathrm{TNSID}}(i\omega) = -\frac{-\omega^2\mu + i\omega(2\zeta_T\omega_1) + \omega_1^2\mu\gamma^2(1+\beta)}{\left\{ \begin{array}{l} \omega^4\mu - i\omega^3[2\omega_1(\zeta_T + \mu\zeta_T + \mu\zeta_1)] - \omega^2\omega_1^2[(\mu + 4\zeta_1\zeta_T) + \mu\gamma^2(1+\mu+\beta)] \\ +i\omega\left[2\omega_1^3(\zeta_T + \mu\gamma^2\zeta_1) + 2\omega_1^3\mu\beta\gamma^2(\zeta_T + \zeta_1)\right] + \omega_1^4\mu\gamma^2(1+\beta+\mu\beta\gamma^2) \end{array} \right\}}. \tag{3}$$

2.2. Equivalent damping ratio of TNSID

Assuming that the seismic ground motion $\ddot{x}_g$ is an ideal white noise process with a constant spectral density of S_0, the mean square displacement response of the primary structure with TNSID could be formulated as [73]:

$$\delta_{x_1}^2 = S_0 \int_{-\infty}^{\infty} \left| H_1^{\mathrm{TNSID}}(i\omega) \right|^2 d\omega = \frac{\pi S_0 \Delta}{2\omega_1^3}, \tag{4}$$

where,

Table 1
Definition of system parameters.

Parameters	Definition
$\omega_1 = \sqrt{k_1/m_1}$	Frequency of the primary structure
$\omega_T = \sqrt{k_T/m_T}$	Frequency of TNSID
$\zeta_1 = c_1/(2m_1\omega_1)$	Damping ratio of the primary structure
$\zeta_T = c_T/(2m_1\omega_1)$	Damping ratio of TNSID
$\mu = m_T/m_1$	Inertia mass ratio of TNSID
$\gamma = \omega_T/\omega_1$	Frequency ratio of TNSID
$\beta = k_{ns}/k_T$	NS ratio of TNSID

$$\Delta = \frac{1}{1+\beta(1+\mu\gamma^2)} \frac{\left\{\begin{array}{l}\mu^4\gamma^4(\zeta_T+\zeta_1+\beta\zeta_1)+\mu^3\gamma^2\zeta_T\left[2\gamma^2(1+\beta)-1\right]\\ +\mu^2\zeta_T\left[\gamma^4(1+\beta)^3+\left(4\gamma^2\zeta_1^2-2\gamma^2\right)(1+\beta)^2+4\gamma^2\zeta_1\zeta_T\left(\beta^2+3\beta+1\right)+4\gamma^2\beta\zeta_T^2+1+\beta\right]\\ +4\mu\zeta_T^2\left[\gamma^2\zeta_1(1+\beta)^2+\zeta_1(1+\beta)+\zeta_T\left(\beta\gamma^2+\beta+1\right)\right]+4\zeta_T^3(1+\beta)\end{array}\right\}}{\left\{\begin{array}{l}\mu^4\gamma^4\zeta_1(\zeta_T+\zeta_1)+2\mu^3\gamma^4\zeta_1\zeta_T+4\mu\zeta_1\zeta_T^2\left[\gamma^2(\beta\zeta_T+\beta\zeta_1+\zeta_1)+\zeta_1+\zeta_T\right]+4\zeta_1\zeta_T^3\\ +\mu^2\zeta_T\left[\gamma^4\zeta_1(1+\beta)^2+\gamma^4\beta^2\zeta_T+2\gamma^2(\beta\zeta_T+\beta\zeta_1+\zeta_1)\left(2\zeta_1^2+2\zeta_1\zeta_T-1\right)+\zeta_1+\zeta_T\right]\end{array}\right\}}. \tag{5}$$

Regarding the vibration control performance of TNSID as the EDR added to the primary structure, an equivalent structure with an enhanced damping ratio $\zeta_e = \zeta_1 + \zeta_s^{\mathrm{TNSID}}$ could be defined, where ζ_s^{TNSID} represents the additional EDR offered by TNSID. Similarly, the mean square displacement response for the equivalent structure could be expressed as [74,75]:

$$\delta_e^2 = \pi S_0/(2\zeta_e\omega_1^3). \tag{6}$$

By aligning the displacement response of the primary structure with TNSID to that of the equivalent structure (i.e., $\delta_{x_1}^2 = \delta_e^2$), ζ_s^{TNSID} could be obtained as:

$$\zeta_s^{\mathrm{TNSID}} = \frac{1}{\Delta} - \zeta_1. \tag{7}$$

It is noted that a larger ζ_s^{TNSID} indicates a better control performance of TNSID for the seismic response of the primary structure.

2.3. Equivalent damping ratio enhancement effect

An essential feature of TID is to improve the control performance of the dashpot element through the inerter element, thus achieving a higher control efficiency. The purpose of introducing the NS element in TNSID is to realize a further enhancement in control efficiency, which will be reflected as a further increment in the EDR of the structure-TNSID system. Furthermore, in comparison to the EDR provided by the dashpot element in TID, the increase in EDR observed for the structure-TNSID system can serve as an indicator of both the EDRE effect of the NS element and the control efficiency of the TNSID. Thus, the EDRE factor can be defined as:

$$G^{\mathrm{TNSID}} = \zeta_s^{\mathrm{TNSID}} - \zeta_T. \tag{8}$$

where ζ_T denotes the damping ratio of TNSID and EDR of the dashpot element. The superior control performance of TNSID compared to the bare dashpot is guaranteed when G^{TNSID} exceeds zero.

3. Parameter optimization of TNSID

In this section, closed-form expressions for the TNSID optimal parameters are proposed to obtain the maximum additional EDR and EDRE factor simultaneously. The influence of TNSID parameters on the additional EDR and EDRE factor are revealed through parametric studies. The superiority of the proposed closed-form expressions is demonstrated by comparing them with the expressions based on the fixed-point strategy. Moreover, a comparison between TNSID and TID is conducted to demonstrate the potential of the NS element in enhancing the control efficiency.

3.1. Closed-form solution of TNSID optimal parameters

Herein, the inertia mass ratio μ and NS ratio β of TNSID should be predetermined, considering the production difficulty and cost of the inerter and NS elements. Obviously, according to the definition of the EDRE factor in Eq. (8), the partial derivatives of ζ_s^{TNSID} and G^{TNSID} are identical with respect to the variables except the damping ratio ζ_T. In other words, the optimal control performance and control efficiency of TNSID could be achieved simultaneously by the same design parameters. Furthermore, EDR is a monotonic function of mass ratio μ and has no extreme points. Therefore, to achieve the maximum additional EDR and EDRE factor simultaneously, the TNSID parameters should yield:

$$\frac{\partial G^{\mathrm{TNSID}}}{\partial\beta} = \frac{\partial\zeta_s^{\mathrm{TNSID}}}{\partial\beta} = 0 \text{ and } \frac{\partial G^{\mathrm{TNSID}}}{\partial\gamma} = \frac{\partial\zeta_s^{\mathrm{TNSID}}}{\partial\gamma} = 0. \tag{9}$$

ζ_s^{TNSID} is selected as the optimization objective to attain the maximum control performance for TNSID. Additionally, G^{TNSID} is adopted as the optimization objective for the highest TNSID control efficiency, aiming to achieve the maximum additional EDR with the lowest damping ratio ζ_T.

Ignoring the inherent damping ratio of the primary structure (i.e., $\zeta_1 = 0$), by solving Eq. (9), the optimal damping ratio of TNSID could be obtained as:

$$\zeta_{T\mathrm{opt1}} = \frac{\mu\gamma}{2(1+\beta+\mu\beta\gamma^2)}\sqrt{\frac{\mu}{2+\mu}(a_4\gamma^4+a_2\gamma^2+a_0)}, \tag{10}$$

where,

$$\begin{cases} a_4 = \beta(1-\mu^2+3\beta+3\beta^2+\beta^3) \\ a_2 = -2(1+\beta)\left[\mu+(1+\beta)^2\right] \\ a_0 = (1+\beta)^2 \end{cases}. \tag{11}$$

Meanwhile, the optimal frequency ratio of TNSID could be obtained as:

$$\gamma_{\text{opt1}} = \sqrt{\frac{-b_1+\sqrt{b_1^2-4b_0b_2}}{2b_2}}, \tag{12}$$

where,

$$\begin{cases} b_2 = \beta\mu^3\left[-2\beta^3(1+\mu)+\beta(6+8\mu+4\mu^2-3\beta\mu)+(4+5\mu)(1+\mu)^2\right] \\ b_1 = \mu^2\left[\begin{matrix}\beta^3(4+6\mu+4\mu^2)+\beta^2(12+16\mu+11\mu^2) \\ +\beta(12+22\mu+18\mu^2+4\mu^3)+(4+4\mu-\mu^2)(1+\mu)^2\end{matrix}\right] \\ b_0 = -2\mu^2(1+\beta)^2(2+2\mu+\mu^2) \end{cases}. \tag{13}$$

It is noted that for stability, the stiffness of the structure-TNSID system must be positive. Therefore, the lower and upper thresholds of the NS ratio β must satisfy Eq. (14) [56].

$$\frac{-1}{1+\mu\gamma^2} < \beta < 0. \tag{14}$$

Given the primary structure information, as shown in Fig. 2, the optimal parameters of TNSID could be preliminarily estimated following the process as follows:

1) Determine the parameters of the primary structure based on the modal analysis, including the generalized mass m_1, frequency ω_1, and damping ratio ζ_1 for the fundamental mode.
2) Assume the inertia mass ratio μ for the inerter element and the NS ratio β for the NS element.
3) calculate the optimal damping ratio ζ_{Topt1} and frequency ratio γ_{opt1} of TNSID using Eqs. (10) and (12).
4) check whether the assumed β is within the reasonable range according to Eq. (14) to ensure that the overall structural stiffness is positive, if β is out of the acceptable range, go back to step 2) and adjust the value of β.
5) If β is within the reasonable range, the inertia mass m_T, stiffness k_T, negative stiffness k_{ns}, and frequency ratio of the TNSID could be preliminarily estimated based on the definitions provided in Table 1. Further detailed design for TNSID and the primary structure could be conducted based on the preliminary estimated parameters.

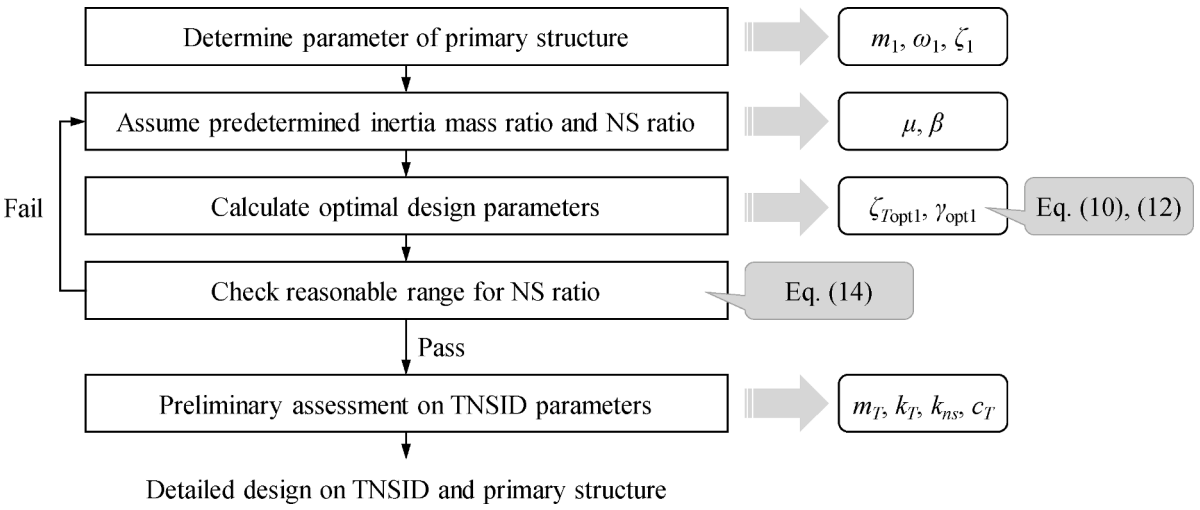

Fig. 2. Flowchart of the TNSID design procedure.

3.2. Parametric study

Considering the feasibility of the device and the adverse effect of excessive low negative stiffness on structural stability, the lower limit of the NS ratio is set to be −0.3 in this study, with reference to the existing studies. The analysis results in Fig. 3 demonstrate the influence of the structural damping ratio ζ_1 on TNSID parameters for an NS ratio $\beta = -0.3$. For the TNSID optimal damping ratio ζ_{Topt1} and optimal frequency ratio γ_{opt1}, the closed-form solutions presented in Eqs. (10) to (14) consistent with the numerical solution when the main structure is undamped (i.e., $\zeta_1 = 0$), which verifies the correctness of the closed-form solutions. Herein, the enumeration optimization method can be utilized to obtain the numerical solution of ζ_{Topt1} and γ_{opt1} to maximize ζ_s^{TNSID} or G^{TNSID}. As observed in Fig. 3, ζ_1 has a minor influence on ζ_{Topt1} and γ_{opt1}, indicating the reasonability of the hypothesis of $\zeta_1 = 0$ for deriving the closed-form solutions. This can also be supported by that the results of EDR ζ_s^{TNSID} and EDRE factor G^{TNSID} based on the closed-form solution agree well with the numerical solution for various ζ_1.

The results presented in Fig. 3(c) demonstrate that ζ_s^{TNSID} exhibits a positive correlation with μ, while a negative correlation with ζ_1. This indicates that increasing the inertia mass ratio enhances the control performance of TNSID, while a larger structural damping ratio weakens it. Fig. 3(d) illustrates a negative correlation between G^{TNSID} and ζ_1, indicating that an increase in the structural damping ratio has an adverse impact on the EDRE effect of TNSID. Moreover, G^{TNSID} exhibits an remarkable upward trend as μ increases when μ is less than 0.1, in which case increasing the inertia mass ratio significantly improves the EDRE effect of TNSID. However, if μ continues to increase, a decrease in G^{TNSID} occurs when $\mu > 0.5$. In particular, G^{TNSID} may become negative when μ is excessively large, which implies that the control performance of TNSID is inferior to that of the bare dashpot; in such cases, utilizing TNSID would be meaningless. In order to fully utilize the EDRE effect with the smallest possible inertia mass, it is recommended that the value of the

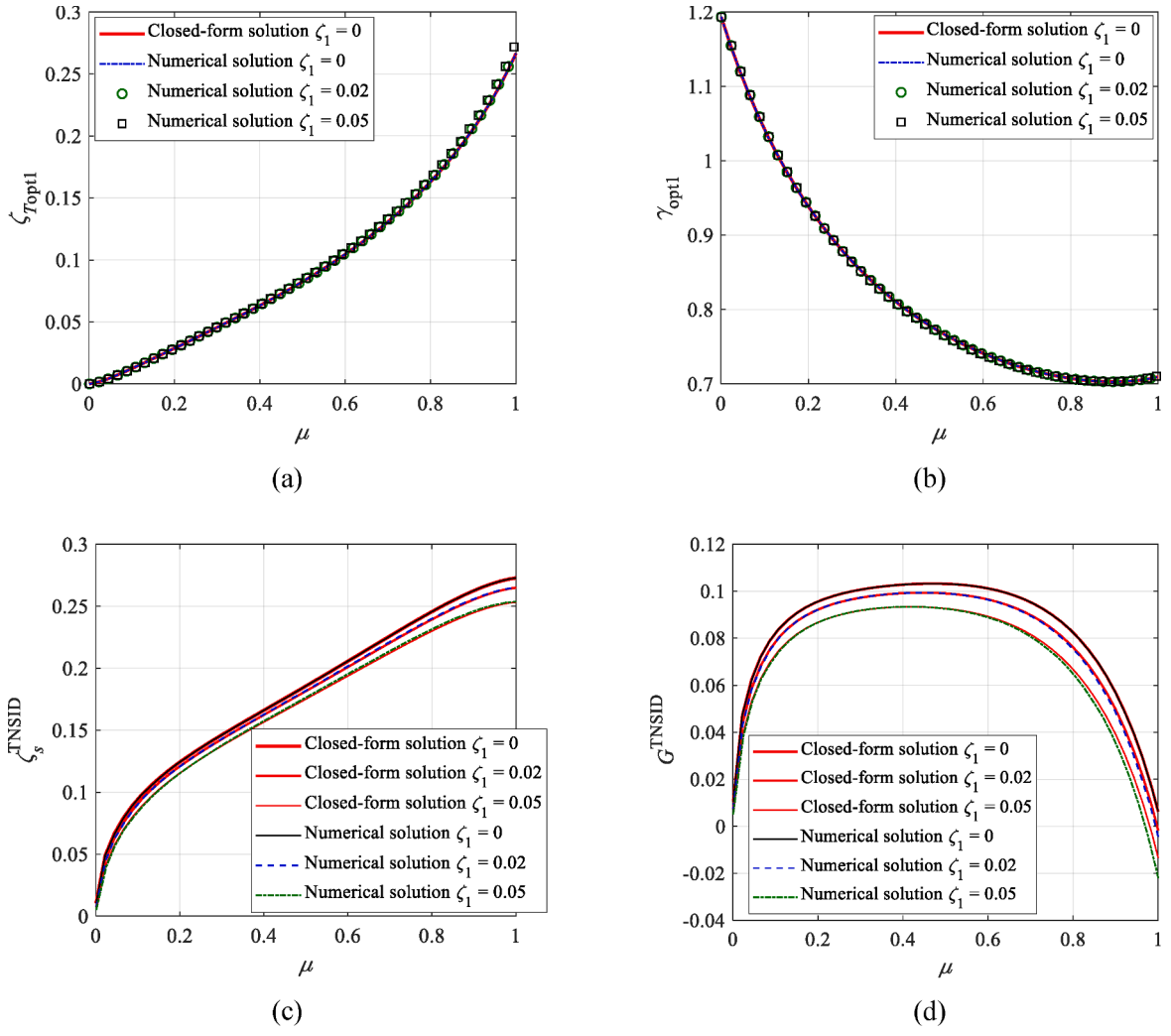

Fig. 3. Influence of structural damping ratio ζ_1 on TNSID parameters for NS ratio $\beta = -0.3$; (a) optimal damping ratio ζ_{Topt1}, (b) optimal frequency ratio γ_{opt1}, (c) additional EDR ζ_s^{TNSID}, and (d) EDRE factor G^{TNSID}.

TNSID inertia mass ratio μ be less than 0.1. Furthermore, in order to avoid the degradation of the EDRE effect, μ should be less than 0.5.

According to the discussion above, it can be concluded that the closed-form solutions of TNSID optimal parameters (i.e., ζ_{Topt1} and γ_{opt1}) are correct. The structural damping ratio exerts a negligible influence on the optimal parameters of TNSID, which supports the reasonability of disregarding this factor in deriving the closed-form solutions. Increasing the inertia mass ratio enhances the control performance of TNSID. In this study, the TNSID inertia mass ratio μ is recommended to be below 0.1 for efficiently utilizing the EDRE effect.

The variation of TNSID parameters with inertia mass ratio μ and NS ratio β for $\zeta_1 =$ 0.02 is prepared, as shown in Fig. 4, where β is assumed to range from 0 to −0.3. An increase in ζ_{Topt1} can be observed as both μ and $|\beta|$ increase, suggesting that the optimal damping ratio of TNSID becomes larger with the increment of inertia mass ratio and absolute value of NS ratio. In addition, the optimal frequency ratio of TNSID increases with the decrease in inertia mass ratio and the increase in absolute value of NS ratio, as observed in Fig. 4(b). It is evident that ζ_s^{TNSID} and G^{TNSID} exhibits a positive correlation with both μ and $|\beta|$. Therefore, the control performance and EDRE effect of TNSID can be improved by increasing the inertia mass ratio and NS ratio.

3.3. Performance comparison

The optimization method of TNSID was previously proposed by Li et al. [56] based on the fixed-point strategy, where the optimal frequency and damping ratios of TNSID are obtained as follows:

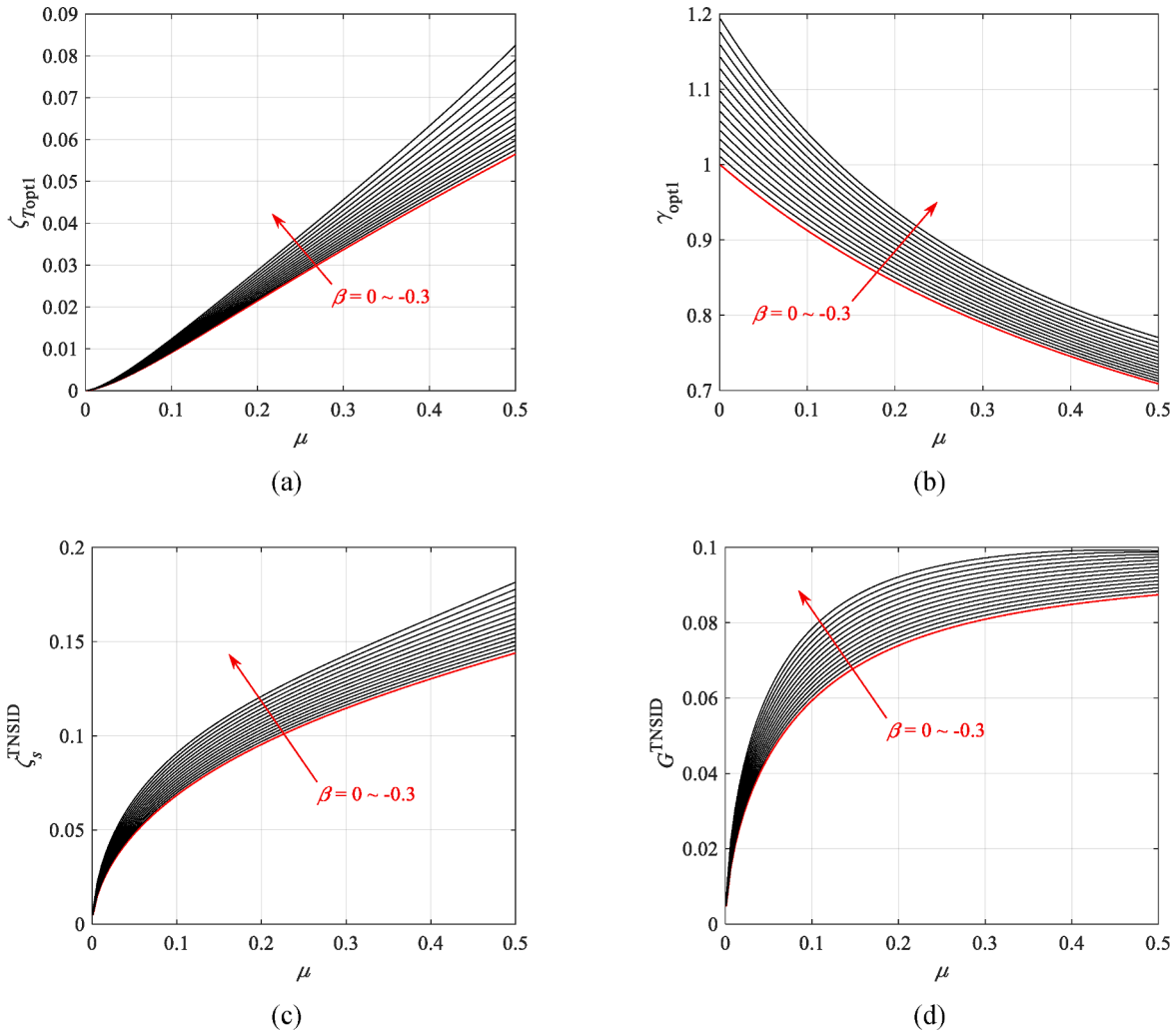

Fig. 4. Variation of TNSID parameters with inertia mass ratio μ and NS ratio β for $\zeta_1 =$ 0.02; (a) optimal damping ratio ζ_{Topt1}, (b) optimal frequency ratio γ_{opt1}, (c) additional EDR ζ_s^{TNSID}, and (d) EDRE factor G^{TNSID}. The red curve represents $\beta = 0$.

$$\gamma_{\text{opt2}} = \sqrt{\frac{1}{(1+\mu)^2+\beta}} \text{ and } \zeta_{\text{opt2}} = \frac{1}{2\mu\gamma}\sqrt{\frac{(3+3\mu+3\beta+2\mu\beta)\mu}{(2+\mu)\beta^2+2\beta(1+\mu)(2+\mu)+2(1+\mu)^2}}. \tag{15}$$

To illustrate the difference between the proposed optimization method based on EDR and the fixed-point strategy-based method, comparison results of the optimal design parameters and performance indicators for TNSID and TID are presented in Figs. 5 and 6. TNSID1 is optimized by the proposed Eqs. (10) to (13), and TNSID2 is optimized according to Eq. (15). Meanwhile, TID1 and TID2 are designed based on the EDR and the fixed-point strategy, respectively.

As illustrated in Fig. 5, the value of γ_{opt} for TNSID1 is close to that of TNSID2 when μ is less than 0.1, whereas γ_{opt} for TNSID1 increasingly surpasses that of TNSID2 when μ exceeds 0.1. The values of $\zeta_{T\text{opt}}$ for TNSID1 and TID1 are comparatively lower than those for TNSID2 and TID2, implying that the proposed method requires a lower optimal damping ratio in comparison to the fixed-point strategy-based method. The values of $\zeta_{T\text{opt}}$ and γ_{opt} for TNSID1 are lower than those for TID1 for a smaller $|\beta|$, and exceeds the values for TID1 as $|\beta|$ increases. It is noted that for $\beta = 0$, the values of $\zeta_{T\text{opt}}$ for TNSID1 and TID1 do not align. This is because the partial differential variable on the left side in Eq. (9) is β, whereas on the left side in Eq. (A7) is μ, which makes the derived expressions for $\zeta_{T\text{opt}}$ different. Meanwhile, the value of $\zeta_{T\text{opt}}$ for TID2 is equal to that of TNSID2 when $\beta = 0$, since the expressions for $\zeta_{T\text{opt}}$ of TNSID2 and TID2 become identical.

The abscissa in Fig. 6 is set as ζ_T to enhance the visibility of the EDRE effect. The additional EDR and EDRE factors for TNSID1 and TID1 exhibit a positive correlation with the damping ratio ζ_T, suggesting that enlarging ζ_T could improve the control performance and control efficiency of both the TNSID1 and TID1 designed by the proposed method. The increase of ζ_T also leads to improvement in the additional EDR and the control performance of TNSID2 and TID2. However, the EDRE factor for TNSID2 and TID2 is positively related to ζ_T only when ζ_T<0.04, in which case the enlargement of ζ_T would be beneficial for enhancing their EDRE effect. As ζ_T continues to increase, the enlargement of ζ_T weakens the EDRE effect of TNSID2 and TID2, and is not beneficial for improving the control efficiency. The additional EDR and EDRE factors for TNSID1 and TNSID2 exhibit positive correlations with $|\beta|$, suggesting that enlarging the NS ratio could also improve the control performance and efficiency of TNSIDs.

From Fig. 6(a), the additional EDR for TNSID1 is larger than that for TID1 except for $|\beta|$ close to zero, and the additional EDR for TNSID2 is always larger than that for TID2. This reveals the potential of the NS element in enhancing the TNSID control performance. In general, the additional EDR for TNSID1 and TID1 surpasses those for TNSID2 and TID2. This highlights the advantage of the proposed optimization method over the fixed-point strategy-based method, in terms of enhancing the control performance. It is noted that the additional EDR for TNSID2 is smaller than that of TID1 when ζ_T is larger than 0.02, indicating that the control performance of the TNSID optimized based on the fixed-point strategy could be smaller than that of the TID with the same ζ_T, even after introducing the NS element. Considering the manufacturing limitations of devices such as fluid dampers, it is recommended to set the damping ratio to be less than 1 %, by which the control efficiency of TNSID1 surpasses the highest possible level of TNSID2 at any value of ζ_T.

In Fig. 6(b), the EDRE factor for TNSID1 is observed to be larger than that of TNSID2, indicating a superior EDRE effect of TNSID1. This is attributed to the fact that the optimal design objective of TNSID1 is to maximize the additional EDR ζ_s^{TNSID} with a minimum damping ratio ζ_T. This trend becomes increasingly significant with the increase of $|\beta|$. Thus, enlarging the NS ratio could further enhance the EDRE effect of TNSID relative to the dashpot element. In conclusion, the utilization of the NS element is highly advantageous in improving both the control performance and control efficiency of the TNSID1 designed by the proposed design method.

To summarize, based on the same damping ratio ζ_T, the TNSID1 optimized using the proposed method could achieve a higher additional EDR and EDRE factor compared to the TNSID2 and TID2 designed by the fixed-point strategy. This highlights the superiority

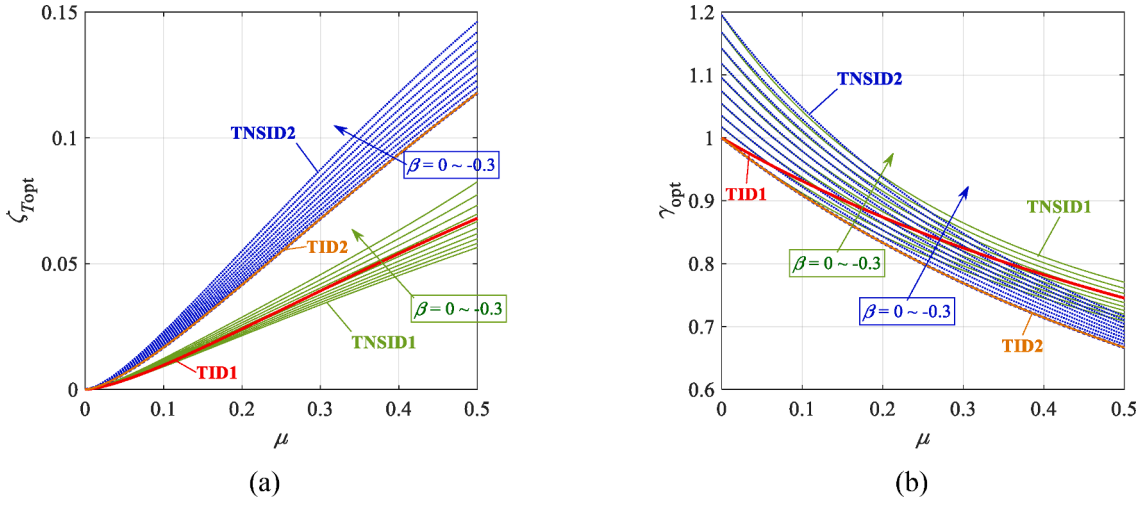

Fig. 5. Comparison results of optimal parameters for TNSIDs and TIDs with the same inertia mass ratio μ; (a) optimal damping ratio $\zeta_{T\text{opt}}$ and (b) optimal frequency ratio γ_{opt}.

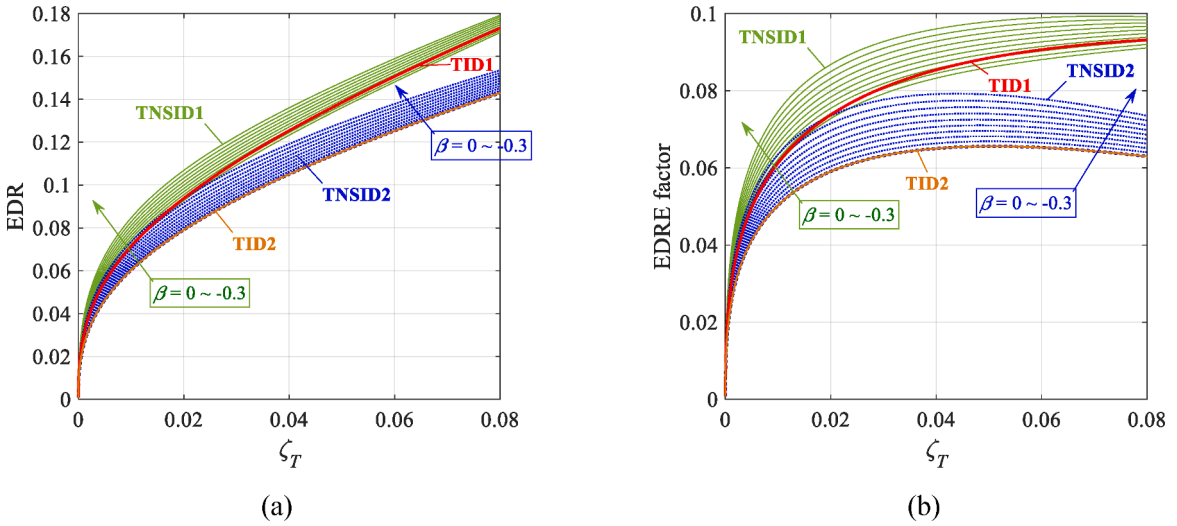

Fig. 6. Comparison results of control performance for TNSIDs and TIDs with the same damping ratio ζ_T; (a) additional EDR and (b) EDRE factor.

of the proposed optimization method and reveals the potential of the NS element in terms of enhancing the control performance and efficiency of TNSID.

4. Validation and implementation of TNSID

In this section, the optimized TNSID is validated and implemented for both SDOF and MDOF structures, utilizing frequency transfer function analysis and time-history analysis to consider harmonic and real seismic ground motions, respectively.

4.1. Performance validation of TNSID for SDOF structures

Considering an SDOF structure with a period of one second and an inherent damping ratio of $\zeta_1 = 0.02$. As the control performance and efficiency of TNSID improve with the increase of $|\beta|$, the NS ratio is taken as -0.3 here to clearly exhibit the difference between TNSID and the devices without NS element and also to highlight the advantages of the proposed optimization method. The damping ratio ζ_T for all the additional devices are assumed to be 0.1 %, 0.3 %, and 0.6 %, the corresponding design parameters of various control devices are listed in Table 2. It is noted that to better illustrate the EDRE effect of TNSIDs and TIDs, this section also presents the design and analysis results of the VD, which has the same damping coefficient as the dashpot element in the TNSID and TID. Herein, the TNSID1 and TID1 are designed by the proposed method based on EDR, while the TNSID2 and TID2 are designed based on the fixed-point strategy.

The displacement frequency transfer functions of the primary structure controlled by each of the devices are presented in Fig. 7. The control frequency band (CFB) of TID2 is regarded as the reference standard for the control bandwidth. It is well known that TID2 is effective in reducing the structural displacement response within the CFB range, while its control performance deteriorates and the

Table 2
Design results of various control devices for SDOF structures.

Devices	Design formula	Parameters	Damping ratio ζ_T		
			$\zeta_T = 0.1\,\%$	$\zeta_T = 0.3\,\%$	$\zeta_T = 0.6\,\%$
TNSID1	Eqs. (10) to (13) (EDR-based)	β	− 0.3	− 0.3	− 0.3
		μ	0.0168	0.0354	0.0581
		γ	1.1647	1.1335	1.0986
TNSID2	Equation (15) (Fixed-point strategy-based)	β	− 0.3	− 0.3	− 0.3
		μ	0.0111	0.0236	0.0378
		γ	1.1766	1.1564	1.1344
TID1	Eq. (A8) (EDR-based)	μ	0.0205	0.0435	0.0705
		γ	0.9849	0.9687	0.9505
TID2	Eq. (A4) (Fixed-point strategy-based)	μ	0.0142	0.0297	0.0480
		γ	0.9860	0.9712	0.9542
VD	Same damping coefficient as TNSIDs and TIDs	ζ_T	0.1 %	0.3 %	0.6 %

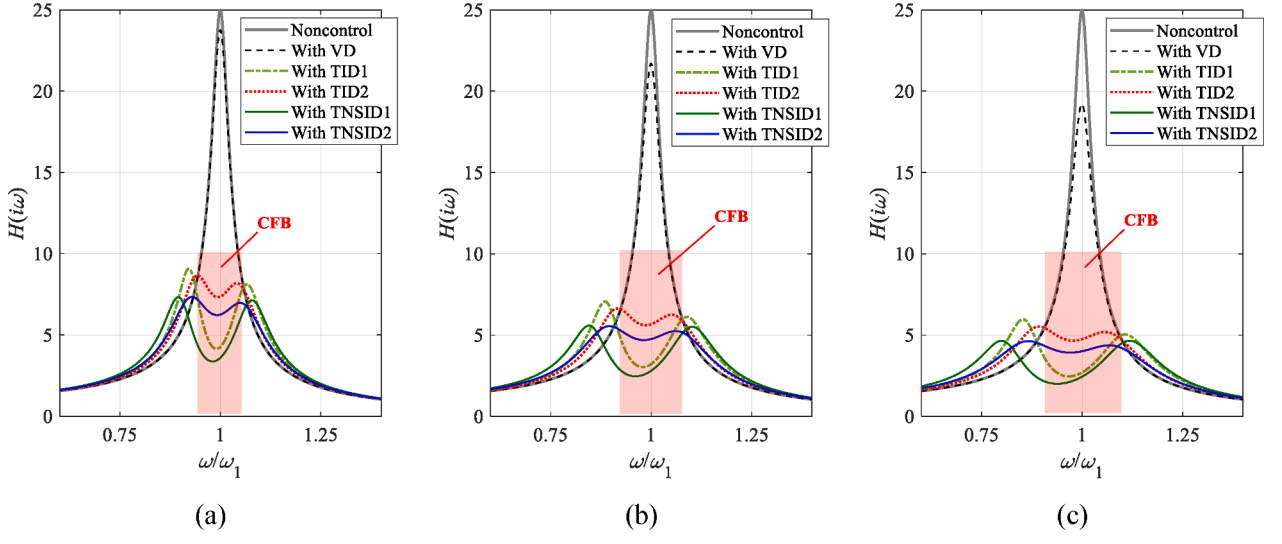

Fig. 7. Displacement frequency transfer functions of the primary structure with various control devices for $\beta = -0.3$ and $\zeta_1 = 0.02$; (a) $\zeta_T = 0.1\,\%$, (b) $\zeta_T = 0.3\,\%$, and (c) $\zeta_T = 0.6\,\%$.

response might even be amplified beyond the CFB range. The expansion of the CFB indicates that the effectiveness of controlling the displacement response of the primary structure under seismic excitations can be enhanced across a wider frequency range.

The frequency transfer function under the control of TID1 is comparatively lower than that of TID2 within the CFB, indicating the superior control performance of TID1 over TID2 within the CFB. However, the control performance of TID1 is inferior to that of TID2 beyond the CFB. The above phenomenon could also be observed between TNSID1 and TNSID2. This verifies that the proposed EDR-based design methodology allows TID1 and TNSID1 to achieve better control performance within the CFB than the corresponding TID2 and TNSID2 designed based on the fixed-point strategy. In addition, with the same values of ζ_T, the frequency transfer functions under the control of the TNSIDs exhibit smaller magnitudes compared to those of TIDs within CFB, thereby demonstrating the potential of the NS element in enhancing the control performance. Moreover, without the inerter and NS elements, the frequency transfer function peaks under the control of VD are significantly higher than those of TNSIDs and TIDs, and when the damping ratio $\zeta_T = 0.1\,\%$, the frequency transfer function of VD almost coincides with that of the noncontrol structure, indicating a poor control performance of VD. Meanwhile, the peak values of TID1 and TNSID1 are only 36 % and 28 % of the noncontrol structure, respectively. It is verified that by using the same ζ_T, the control efficiency of TID1 is significantly improved, while that of TNSID1 is further enhanced by introducing the NS element. Obviously, the control efficiencies of TID1 and TNSID1 also surpass those of TID2 and TNSID2, which are designed using the fixed-point strategy.

Compared to the harmonic seismic excitations considered in the frequency transfer function analysis, the actual seismic excitations exhibit greater complexity and randomness in the frequency components and spectral distributions. Under seismic excitations with different spectral characteristics, to assess the robustness of the trends reflected by the above frequency transfer functions, further investigations were carried out by time history analysis to compare the control performance of different devices based on different optimization methodologies. Based on the spectral characteristics of twenty ground motion records suggested by FEMA-440 [76], two groups of ten records each were created. Table 3 presents comprehensive information for each ground motion, while Fig. 8 illustrates the velocity spectra and their corresponding averages for the two groups of ground motions with a damping ratio of 2 %. The dominant frequencies in the velocity spectra for the first group of ground motions are predominantly centered around 0.5 seconds (referred to as the SP group), whereas for the second group, they exhibit a pronounced concentration around 1.0 seconds (referred to as the LP group). These two groups represent two types of ground motions with different spectral distribution patterns and predominant periods.

Meanwhile, SDOF primary structures with periods of 0.5s, 1.0s, and 2.0s are considered to represent short-, medium-, and long-period structures respectively. The mean response reduction factors (RRFs) of the three SDOF structures by supplementing TNSIDs, TIDs, and VDs are shown in Figs. 9 and 10. The RRF for the three devices under the i-th ground motion is defined as

$$ {}_{\mathrm{TNSID1}}\mathrm{RRF} = \frac{{}_{\mathrm{NC}}d_{p,i} - {}_{\mathrm{TNSID1}}d_{p,i}}{{}_{\mathrm{NC}}d_{p,i}}, \quad {}_{\mathrm{TID1}}\mathrm{RRF} = \frac{{}_{\mathrm{NC}}d_{p,i} - {}_{\mathrm{TID1}}d_{p,i}}{{}_{\mathrm{NC}}d_{p,i}}, \quad {}_{\mathrm{VD1}}\mathrm{RRF} = \frac{{}_{\mathrm{NC}}d_{p,i} - {}_{\mathrm{VD1}}d_{p,i}}{{}_{\mathrm{NC}}d_{p,i}}, \tag{16} $$

where ${}_{\mathrm{TNSID1}}d_{p,i}$, ${}_{\mathrm{TID1}}d_{p,i}$, and ${}_{\mathrm{VD1}}d_{p,i}$ denote the peak displacement responses of structures with the three devices under the i-th ground motion. TNSID1 and TID1 are designed using the proposed optimization methodology based on EDR. The damping coefficient of VD1 is the same as that of TNSID1. ${}_{\mathrm{NC}}d_{p,i}$ denotes the peak displacement response of the noncontrol structure under the same ground motion. When varying the inertia mass ratio μ, the parameters of TNSID1, TID1, and VD1 could be determined separately. Time history analyses were performed on both the controlled and noncontrol structures, by inputting the two groups of ground motions. For each group, mean values of the RRFs in Eq. (16) were obtained statistically. As depicted in Figs. 9 and 10, given the different structural periods and spectral characteristics of the ground motions, the control performance of TNSID1 is significantly better than that of VD1, indicating that the TNSID1 designed by the proposed methodology can achieve superior control efficiency. Moreover, it is demonstrated that the control performance of TNSID1 is consistently better than that of TID1 under the ground motions with different spectral characteristics, indicating that the additional NS further improves the control performance of TID.

Table 3
Utilized ground motion records adopted from Appendix C of FEMA-440.

SP group				LP group			
Name	Magnitude (Ms)	Station Number	PGA(cm/s^2)	Name	Magnitude (Ms)	Station number	PGA(cm/s^2)
Northridge	6.8	24399	228.5	Loma Prieta	7.1	1590	134.7
Whittier Narrows	6.1	141	133.8	Loma Prieta	7.1	1590 (USGS)	94.6
Imperial Valley	6.8	286	189.2	Loma Prieta	7.1	1002 (USGS)	270
San Fernando	6.5	269	133.4	Loma Prieta	7.1	1002 (USGS)	222
Loma Prieta	7.1	58135	433.1	Loma Prieta	7.1	58117	112
Morgan Hill	6.1	47006	95	Loma Prieta	7.1	1662 (USGS)	254.7
Northridge	6.8	90021	393.3	Loma Prieta	7.1	58223	231.5
Loma Prieta	7.1	47381	531.7	Loma Prieta	7.1	58472	281.4
Imperial Valley	6.8	5053	269.6	Loma Prieta	7.1	58224	191.3
Morgan Hill	6.1	57425	183	Loma Prieta	7.1	58224	239.4

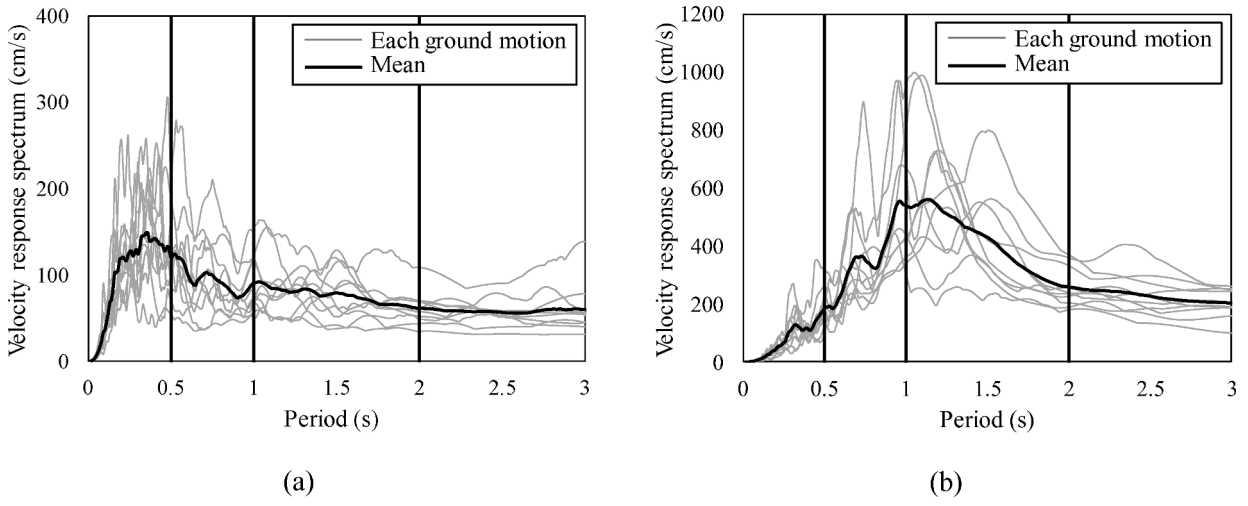

Fig. 8. Velocity response spectra at damping ratio of 2 % for ground motions of (a) SP group and (b) LP group.

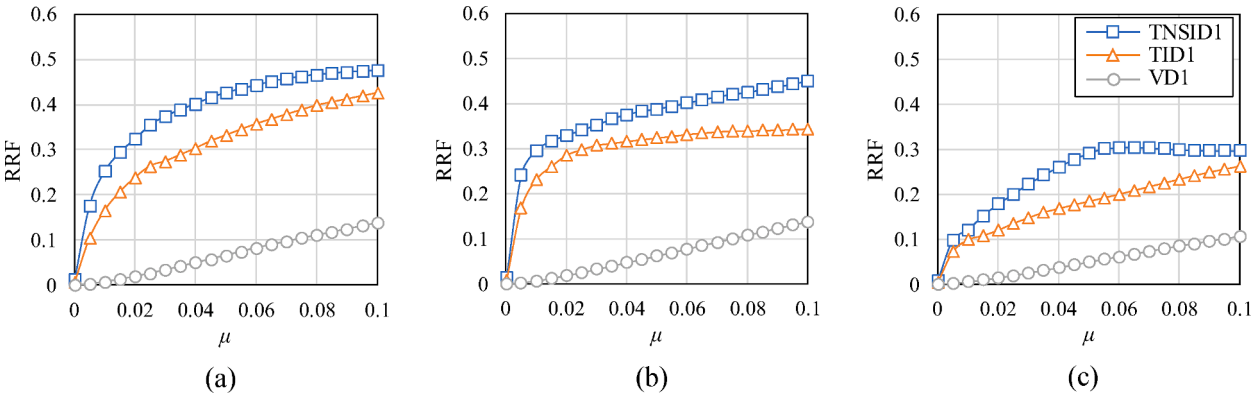

Fig. 9. Response reduction factor (RRF) of SDOF structures achieved by various devices under SP group of ground motions, considering structural periods as (a) 0.5 s, (b) 1.0 s, and (c) 2.0 s.

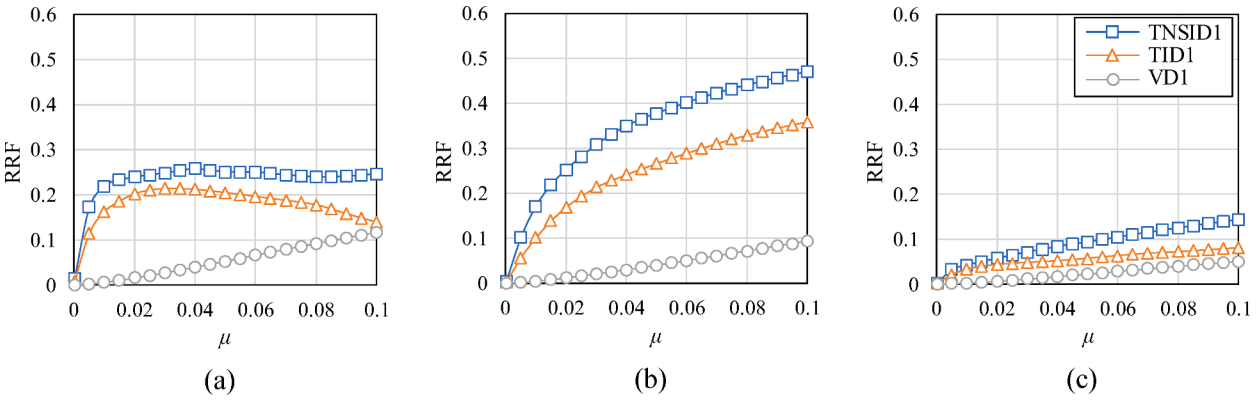

Fig. 10. Response reduction factor (RRF) of SDOF structures achieved by various devices under LP group of ground motions, considering structural periods as (a) 0.5 s, (b) 1.0 s, and (c) 2.0 s.

Moreover, for the first group of seismic motions, when the structural period is 0.5 s, the superiority of the control performance of TNSID1 relative to TID1 is more evident. Similarly, TNSID1 shows a more significant control performance than TID1 for the second group of seismic motions, when the structural period is 1.0 s. This indicates that the enhancement effect of NS on the control

performance of TID is influenced by the spectral characteristics of the ground motion. The enhancement effect is even more significant when the dominant period of the velocity spectrum is close to the structural period.

The mean control efficiency indices (CEIs) of TNSID1 and TNSID2 on the three SDOF structures are compared in Figs. 11 and 12. TNSID1 and TNSID2 were designed by the proposed optimization methodology based on EDR and fixed-point strategy, respectively. Under the i th ground motion, the CEI of TNSID1 and TNSID2 are defined as

$$_{\text{TNSID1}}\text{CEI} = \frac{_{\text{VD1}}d_{p,i}}{_{\text{TNSID1}}d_{p,i}}, \quad _{\text{TNSID2}}\text{CEI} = \frac{_{\text{VD2}}d_{p,i}}{_{\text{TNSID2}}d_{p,i}}, \tag{17}$$

where $_{\text{TNSID1}}d_{p,i}$ and $_{\text{TNSID2}}d_{p,i}$ denote the peak displacement responses of the SDOF structures controlled by the TNSID1 and TNSID2 under the i-th ground motion, respectively. $_{\text{VD1}}d_{p,i}$ and $_{\text{VD2}}d_{p,i}$ denote the peak displacement responses of the SDOF structures with VD1 and VD2, which have the same damping ratios as TNSID1 and TNSID2, respectively. Time history analyses were performed on the SDOF structures with and without dampers by inputting the two groups of ground motions. For each group, CEIs were calculated by Eq. (17), and the mean values were obtained statistically. As depicted in Figs. 11 and 12, for structures with varying periods and ground motions with different spectral characteristics, the control efficiency of TNSID1 is higher than that of TNSID2. That is to say, compared to the optimization method based on the fixed-point strategy, the proposed optimization method enables TNSID to enhance the control performance of VD to a higher level, while TNSID and VD have the same damping ratio. Similar to Figs. 9 and 10, when the structural period is close to the dominant period of the ground motion velocity spectrum, the advantage of the proposed optimization method in terms of control efficiency is more significant, and the mean CEI of TNSID1 is more evidently higher than that of TNSID2.

According to the time history analysis results above, the superiority of the proposed methodology and the potential of the NS element in enhancing the control performance and efficiency of TNSID are verified. The enhancement effect is robust for structures with different periods and ground motions with different spectral characteristics. The enhancement effect becomes more evident when the structural period is close to the predominant period of the ground motion.

4.2. Implementation of TNSID for an MDOF structure

The MDOF model [56,71,77,78] shown in Fig. 13 for a five-story steel structure is utilized to investigate the implementation of TNSID in the building structure. The first three periods of this building are 0.992 s, 0.354 s, and 0.223 s. The vibration control performance of TNSID, TID, and VD are compared. Note that all the control devices are assumed to be installed on the first story to eliminate any potential impact from the device location.

The optimization methodologies for the devices could be applied to the MDOF structure by simplifying it into an equivalent SDOF structure based on the fundamental mode. By suppressing the fundamental modal response, it is possible to maximize the control performance of the devices [e.g. 25,26,56]. Considering ζ_T = 0.1 %, 0.3 %, 0.6 %, and $\beta = -0.3$, the optimal design results for the TNSIDs and TIDs could be provided in Table 4, based on the optimal results in Table 2, together with the natural frequency and generalized mass of the fundamental mode. It is noted that in this study, the damping coefficient of the control devices is considered to be the main limiting factor in the design parameters considering the limitations of the production process. Therefore, the optimization objective of TNSID is to achieve the best control performance with the lowest damping coefficient, that is to realize the best control efficiency while considering the engineering feasibility. In Table 4, the maximum damping coefficient for the control devices is 750.14 kN•s/m, which is considered to be physically achievable for real devices such as a fluid damper.

Fig. 14 shows the mean peak interstory drift angle (IDA) response of the primary structure controlled by various devices under the ten ground motions of the LP group. The results demonstrate that both TNSIDs and TIDs exhibit superior control performance than VDs, indicating a significant EDRE effect. The control performance of TID1 and TNSID1 are better than those of TID2 and TNSID2, respectively. It verifies the advantages of the proposed EDR-based design methodology over the fixed-point strategy-based method.

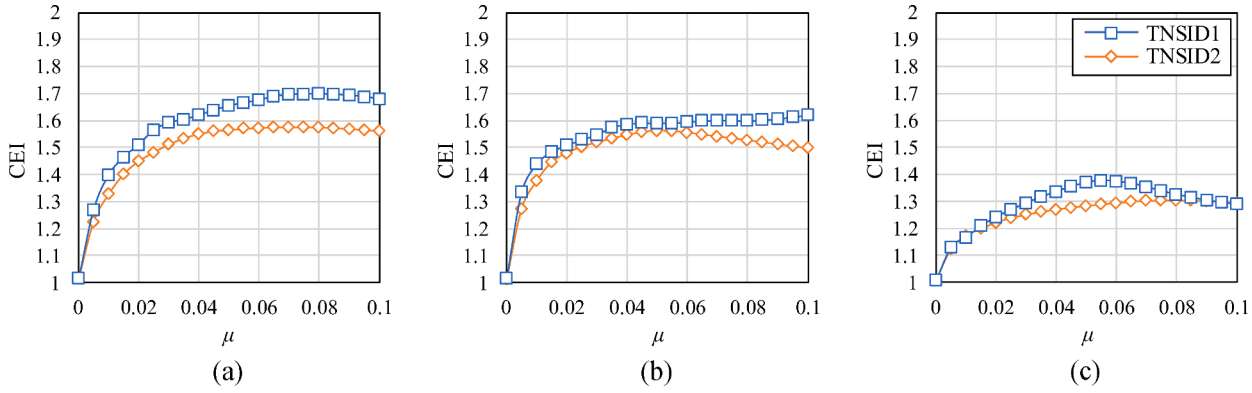

Fig. 11. Control efficiency index (CEI) of SDOF structures achieved by various devices under SP group of ground motions, considering structural periods as (a) 0.5 s, (b) 1.0 s, and (c) 2.0 s.

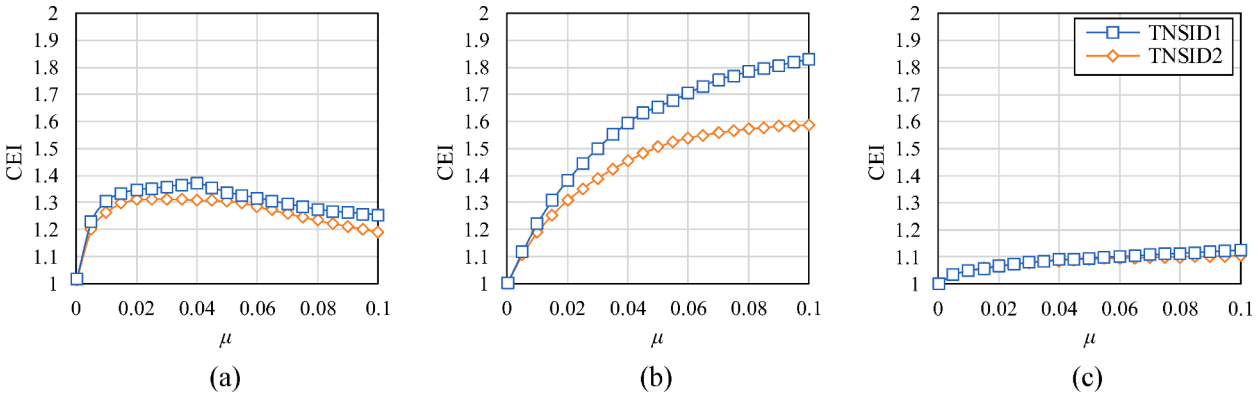

Fig. 12. Control efficiency index (CEI) of SDOF structures achieved by various devices under LP group of ground motions, considering structural periods as (a) 0.5 s, (b) 1.0 s, (c) 2.0 s.

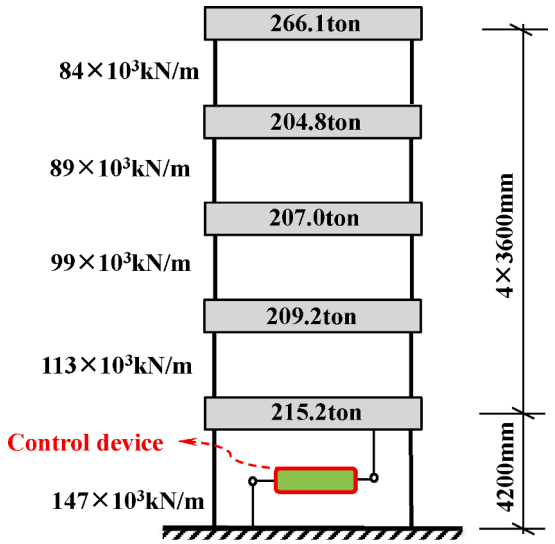

Fig. 13. MDOF model of the Kajima-Shizuoka building.

Table 4
Design results of various control devices when $\beta = -0.3$.

Devices	Design formula	Parameters	Damping ratio ζ_T		
			$\zeta_T = 0.1\%$	$\zeta_T = 0.3\%$	$\zeta_T = 0.6\%$
TNSID1	Eqs. (10) to (13) (EDR-based)	c_T ($\times 10^2$ kN•s/m)	1.3016	3.7834	7.5014
		m_T ($\times 10^5$ kg)	1.6473	3.4710	5.6968
		k_T ($\times 10^4$ kN/m)	0.8967	1.7895	2.7592
		k_{ns} ($\times 10^3$ kN/m)	−2.6900	−5.3684	−8.2775
TNSID2	Eq. (15) (Fixed-point strategy-based)	c_T ($\times 10^2$ kN•s/m)	1.3016	3.7834	7.5014
		m_T ($\times 10^5$ kg)	1.0884	2.3140	3.7063
		k_T ($\times 10^4$ kN/m)	0.6046	1.2418	1.9141
		k_{ns} ($\times 10^3$ kN/m)	−1.8139	−3.7254	−5.7422
TID1	Eq. (A8) (EDR-based)	c_T ($\times 10^2$ kN•s/m)	1.3016	3.7834	7.5014
		m_T ($\times 10^5$ kg)	2.0100	4.2652	6.9126
		k_T ($\times 10^4$ kN/m)	0.7825	1.6060	2.5059
TID2	Eq. (A4) (Fixed-point strategy-based)	c_T ($\times 10^2$ kN•s/m)	1.3016	3.7834	7.5014
		m_T ($\times 10^5$ kg)	1.3923	2.9121	4.7064
		k_T ($\times 10^4$ kN/m)	0.5470	1.1021	1.7196
VD	Same damping coefficient as TNSIDs and TIDs	c_T ($\times 10^2$ kN•s/m)	1.3016	3.7834	7.5014

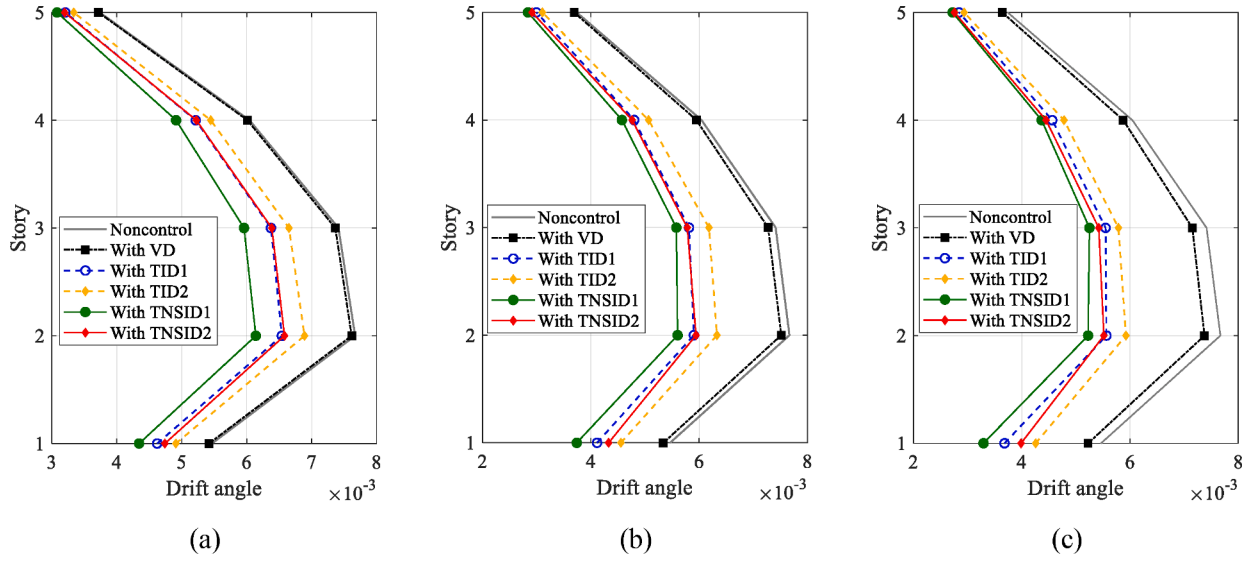

Fig. 14. Mean peak interstory drift angle (IDA) of noncontrol and controlled primary structures under LP group of ground motions, while damping ratios of devices are equally set as (a) $\zeta_T = 0.1\,\%$, (b) $\zeta_T = 0.3\,\%$, and (c) $\zeta_T = 0.6\,\%$.

The control efficiency of TNSID1 is improved compared to TID1, demonstrating the enhancement effect of the NS element.

Fig. 15 shows the mean RRF of the peak IDA responses of the primary structure under the control of the various devices, while the ten LP ground motions are considered. For all the values of ζ_T and all the stories, the RRFs of TNSIDs and TIDs are significantly higher than those of VDs, confirming the high control efficiency resulting from the inerter and NS elements. Furthermore, benefiting from the additional NS elements and the proposed EDR-based optimization method, the RRFs under the control of TNSID1 are always the largest, implying the maximum control performance. With the same NS element, TNSID2 optimized using the fixed-point strategy has a lower RRF compared to TNSID1. For the lower floors, the control performance of TNSID2 could be even lower than that of the TID optimized based on EDR, indicating that the enhancement effect of the NS element has not been fully utilized. It is also observed that the TNSID1 and TID1 optimized using the proposed EDR-based method achieve the maximum RRF at the bottom story where the devices are located, and this trend becomes more evident with the increase of the damping ratio ζ_T. Whereas, for the TNSID2 and TID2 optimized based on the fixed-point strategy, the effect of the device position on the control performance of the interstory drift response

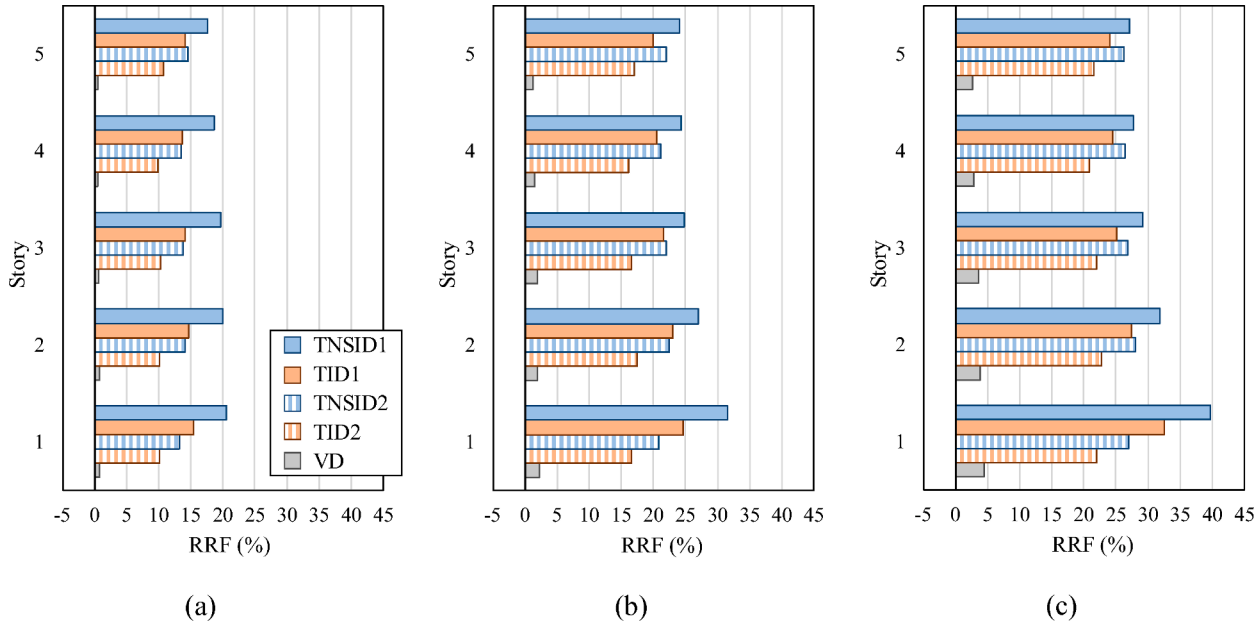

Fig. 15. Mean RRF of peak IDA of primary structure under LP group of ground motions, while damping ratios of devices are equally set as (a) $\zeta_T = 0.1\,\%$, (b) $\zeta_T = 0.3\,\%$, and (c) $\zeta_T = 0.6\,\%$.

is not so obvious.

Fig. 16 shows the mean peak IDA responses of the primary structure under the control of the various devices. The interstory deformation distributions of the noncontrol structure obviously differ from those under the LP ground motions. This is because the fundamental period of the primary structure is about one second, whereas the peak spectral values of the SP ground motions are around 0.5 s, and the higher-order modal response of the structure is more likely to be amplified. For the lower stories, the RRFs under the control of TNSID1 are almost equal to those of TNSID2 and TID1, indicating that the proposed EDR-based design methodology and the additional NS element do not enhance the control performance and efficiency significantly. For the upper floors, such enhancement effect becomes more obvious when the damping ratio is equal to 0.1 %. Therefore, the advantages of the proposed design methodology and NS elements under the excitation of the SP group of ground motions are not evident in general, compared to the LP group of ground motions. By comparing the results in Fig. 14, the law revealed in Section 4.1 is verified, i.e., when the structural fundamental period is close to the predominant period of the ground motion, it is beneficial to utilize the advantages of the proposed design methodology and the additional NS element. When the fundamental period deviates from the ground motion predominant period, these advantages become less significant, and this change is more remarkable for the MDOF primary structure. Nevertheless, the high control efficiency of TNSID1 is still noticeable compared to the VD with the same damping ratio. Meanwhile, there is no significant inferiority of TNSID1 compared to TNSID2, TID1, and TID2 in all cases.

Fig. 17 presents the mean RRF of the peak IDA response of the primary structure with the various devices, while the ten ground motions of the SP group are considered. For different values of the damping ratio ζ_T, control performance at the third and fourth stories is relatively better. This could be explained by the fact that the TNSIDs and TIDs are more effective in controlling the response near the predominant period of the ground motion, the predominant period of the SP ground motions is close to the higher-order modes of the structure, whereas the IDA response at the third and fourth stories are mainly governed by the higher-order modes. This difference between the stories tends to decrease with the increase of ζ_T. When $\zeta_T = 0.1\,\%$, The control performance of TNSID1 surpasses that of both TNSID2 and TID1 across all the stories, demonstrating the advantages of the proposed EDR-based design methodology and the additional NS element in enhancing the control performance and control efficiency.

5. Conclusions

In this study, the EDR-oriented investigation on TNSID is conducted for seismic application. The EDR-based design methodology is proposed to obtain the closed-form solution for the optimal design parameters. The benefits of the proposed EDR-based design methodology and the additional NS element in enhancing the control performance and efficiency of TNSID are validated. The main conclusions can be summarized as follows.

1) The closed-form solution for the optimal parameters of TNSID is proposed by ignoring the inherent damping of the primary structure to simultaneously maximize the additional EDR and EDRE factors. The optimal control performance and control efficiency of TNSID can be consequently achieved. Note that the inherent damping of the primary structure exerts a negligible influence on the optimal parameters of TNSID, which supports the reasonability of disregarding this factor in the derivation process.

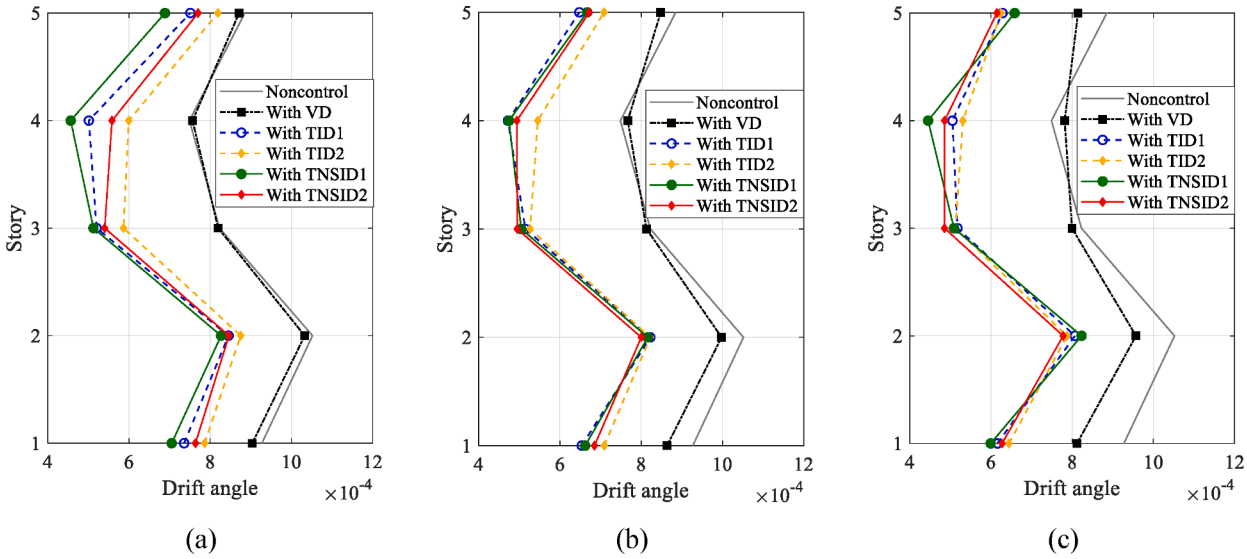

Fig. 16. Mean peak IDA of noncontrol and controlled primary structures under SP group of ground motions, while damping ratios of devices are equally set as (a) $\zeta_T = 0.1\,\%$, (b) $\zeta_T = 0.3\,\%$, and (c) $\zeta_T = 0.6\,\%$.

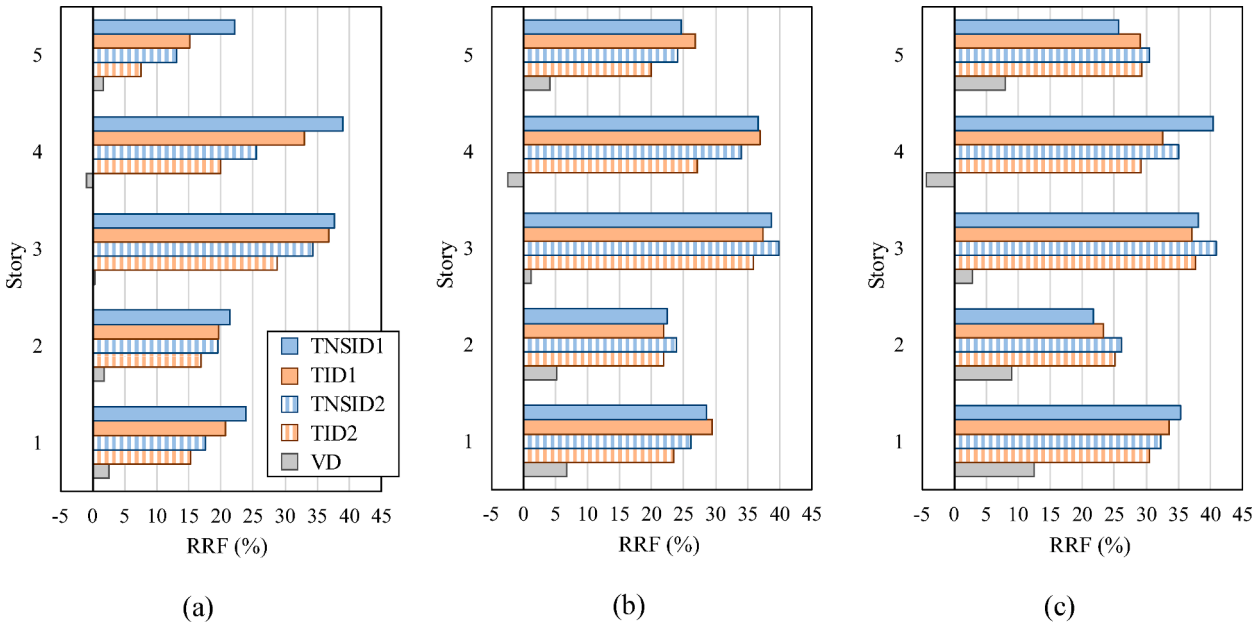

Fig. 17. Mean RRF of peak IDA of primary structure under SP group of ground motions, while damping ratios of devices are equally set as (a) $\zeta_T = 0.1\,\%$, (b) $\zeta_T = 0.3\,\%$, and (c) $\zeta_T = 0.6\,\%$.

2) For the preferable efficiency of the EDRE effect, it is advisable to maintain the TNSID inertia mass ratio below 0.5. Moreover, the proposed EDR-based design methodology ensures that TNSID achieves superior control performance compared to VD, particularly under restricted conditions where the damping ratio is less than 1 %.
3) The comparison results of the optimal additional EDR and EDRE factor between TNSIDs and TIDs reveal that the additional NS element in TNSID leads to enhanced control performance and efficiency compared to TID. Furthermore, this enhancement effect becomes more pronounced with increasing NS ratio.
4) The advantages of the proposed EDR-based design methodology and the additional NS element in enhancing the control performance and efficiency of TNSID are influenced by the spectral characteristics of the ground motions. These advantages can be better realized when the predominant period of the ground motion is close to the fundamental period of the structure.

It is noted that the optimal design of other inerter-based dampers (e.g., TVMD) with negative stiffness is also of utmost importance, which needs to be investigated following the EDR-based design methodology in the future.

CRediT authorship contribution statement

Hui He: Conceptualization, Methodology, Writing – original draft, Investigation. **Linfei Hao:** Conceptualization, Methodology, Writing – review & editing, Investigation. **Yun Zhou:** Conceptualization. **Zicong Lin:** Writing – original draft. **Yue Xiang:** Methodology, Writing – review & editing. **Yafeng Li:** Methodology, Writing – review & editing.

Declaration of competing interest

The authors declare that they have no known competing financial interests or personal relationships that could have appeared to influence the work reported in this paper.

Data availability

Data will be made available on request.

Acknowledgments

This study is supported by the National Key R&D Project of China (No. 2021YFE0112200); the Natural Science Foundation of Hunan Province, China (No. 2024JJ6198; 2024JJ7120); the Scientific Research Project of Hunan Education Department, China (No. 22B0858; 23A0628); the Natural Science Foundation of Guangdong Province, China (No. 2023A1515012516); the Science and

Technology Innovation Project of Hengyang City, China (No. 202250045150).

Appendix: Design criterion of TID

Fig. 1(a) shows the analytical model for the SDOF structure-TID system. The governing equations of motion for the TID-structure system subjected to the seismic ground motion $\ddot{x}_g$ could be written as:

$$\begin{bmatrix} m_1+m_T & -m_T \\ -m_T & m_T \end{bmatrix}\begin{Bmatrix} \ddot{x}_1 \\ \ddot{x}_T \end{Bmatrix}+\begin{bmatrix} c_1 & 0 \\ 0 & c_T \end{bmatrix}\begin{Bmatrix} \dot{x}_1 \\ \dot{x}_T \end{Bmatrix}+\begin{bmatrix} k_1 & 0 \\ 0 & k_T \end{bmatrix}\begin{Bmatrix} x_1 \\ x_T \end{Bmatrix}=-\begin{Bmatrix} m_1 \\ 0 \end{Bmatrix}\ddot{x}_g. \tag{A1}$$

With identical system parameters definition of TID to those of TNSID, Eq. (A1) is rewritten as:

$$\begin{bmatrix} 1+\mu & -\mu \\ -\mu & \mu \end{bmatrix}\begin{Bmatrix} \ddot{x}_1 \\ \ddot{x}_T \end{Bmatrix}+\begin{bmatrix} 2\zeta_1\omega_1 & 0 \\ 0 & 2\zeta_T\omega_1 \end{bmatrix}\begin{Bmatrix} \dot{x}_1 \\ \dot{x}_T \end{Bmatrix}+\begin{bmatrix} \omega_1^2 & 0 \\ 0 & \mu\gamma^2\omega_1^2 \end{bmatrix}\begin{Bmatrix} x_1 \\ x_T \end{Bmatrix}=-\begin{Bmatrix} 1 \\ 0 \end{Bmatrix}\ddot{x}_g. \tag{A2}$$

Consequently, the displacement frequency transfer function of the primary structure under the control of TID is derived as:

$$H_1^{\mathrm{TID}}(i\omega)=\frac{\mu\omega^2-i\omega(2\zeta_T\omega_1)-\mu\gamma^2\omega_1^2}{\left\{\begin{array}{l}-i\omega^3[2\omega_1(\mu\zeta_T+\mu\zeta_1+\zeta_T)]-\omega^2\left[\omega_1^2(\mu+\mu^2\gamma^2+\mu\gamma^2+4\zeta_1\zeta_T)\right] \\ +i\omega\left[2\omega_1^3(\mu\gamma^2\zeta_1+\zeta_T)\right]+\mu\gamma^2\omega_1^4+\mu\omega^4\end{array}\right\}}. \tag{A3}$$

According to the fixed-point strategy, to minimize the peak value of the displacement frequency transfer function, the closed-form expressions of optimal frequency ratio and damping ratio of TID could be respectively expressed as:

$$\gamma_{\mathrm{opt3}}=\frac{1}{1+\mu}\ \text{and}\ \zeta_{T\mathrm{opt3}}=\sqrt{\frac{3\mu^3}{8(1+\mu)^3}}. \tag{A4}$$

Assuming that the seismic excitations are the ideal white noise process, the additional EDR of TID could be obtained as:

$$\zeta_s^{\mathrm{TID}}=\frac{\left\{\begin{array}{l}2\mu^3\gamma^4\zeta_1\zeta_T+\mu^2\zeta_T\left[\zeta_T+\zeta_1+\gamma^2\zeta_1\left(4\zeta_1\zeta_T+4\zeta_1^2-2+\gamma^2\right)\right] \\ +4\mu\zeta_1\zeta_T^2\left(\zeta_T+\zeta_1+\gamma^2\zeta_1\right)+4\zeta_1\zeta_T^3+\mu^4\gamma^4\left(\zeta_1^2+\zeta_1\zeta_T\right)\end{array}\right\}}{\left\{\begin{array}{l}\mu^4\gamma^4(\zeta_T+\zeta_1)+4\mu\zeta_T^2\left[\zeta_1+\zeta_T+\gamma^2\zeta_1\right]+\mu^3\gamma^2\zeta_T(2\gamma^2-1) \\ +\mu^2\zeta_T\left[1-2\gamma^2+\gamma^4+4\gamma^2\left(\zeta_1^2+\zeta_1\zeta_T\right)\right]+4\zeta_T^3\end{array}\right\}}-\zeta_1. \tag{A5}$$

Thus, the EDRE factor of TID is expressed as:

$$G^{\mathrm{TID}}=\zeta_s^{\mathrm{TID}}-\zeta_T. \tag{A6}$$

Similarly, to ensure that the maximum additional EDR and the optimal EDRE effect are achieved simultaneously, TID parameters should yield:

$$\frac{\partial G^{\mathrm{TID}}}{\partial\mu}=\frac{\partial\zeta_s^{\mathrm{TID}}}{\partial\mu}=0\ \text{and}\ \frac{\partial G^{\mathrm{TID}}}{\partial\gamma}=\frac{\partial\zeta_s^{\mathrm{TID}}}{\partial\gamma}=0. \tag{A7}$$

By solving Eq. (A7), the closed-form expressions of optimal frequency ratio and damping ratio should be [74]:

$$\gamma_{\mathrm{opt4}}=\frac{\sqrt{1+\mu/2}}{1+\mu}\ \text{and}\ \zeta_{T\mathrm{opt4}}=\sqrt{\frac{\mu^3}{8(1+\mu)^3}}. \tag{A8}$$

References

[1] J.T. Yao, Concept of structural control, J. Struct. Div.–ASCE 98 (1972) 1567–1574, https://doi.org/10.1061/JSDEAG.0003280.
[2] G. Housner, L.A. Bergman, T.K. Caughey, A.G. Chassiakos, R.O. Claus, Structural control: past, present, and future, J. Eng. Mech. 123 (1997) 897–971, https://doi.org/10.1061/(ASCE)0733-9399(1997)123:9(897).
[3] B.F. Spencer Jr, S. Nagarajaiah, State of the art of structural control, J. Struct. Eng. 129 (2003) 845–856, https://doi.org/10.1061/(ASCE)0733-9445(2003)129:7(845).
[4] E.J. Nielsen, M.L. Lai, T.T. Soong, J.M. Kelly, Viscoelastic damper overview for seismic and wind applications, Smart Struct. Mater: Passive Damping and Isolation, SPIE 2720 (1996) 138–144, https://doi.org/10.1117/12.239081.
[5] A. Wada, Y.H. Huang, M. Iwata, Passive damping technology for buildings in Japan, Prog. Struct. Eng. Mater. 2 (2000) 335–350, https://doi.org/10.1002/1528-2716(200007/09)2:3<335::AID-PSE40>3.0.CO;2-A.
[6] M.D. Symans, F.A. Charney, A.S. Whittaker, M.C. Constantinou, C.A. Kircher, Energy dissipation systems for seismic applications: current practice and recent developments, J. Struct. Eng. 134 (2008) 3–21, https://doi.org/10.1061/(ASCE)0733-9445(2008)134:1(3).

[7] S. Hikone, R. Kidokoro, K. Ohara, Applications of Hysteretic Steel Dampers in Buildings of Novel Feature, in: Proceedings of the 14th World Conference on Earthquake Engineering, Beijing, 2008.
[8] T. Nakai, H. Kurino, T. Yaguchi, K. Naoki, Control effect of large tuned mass damper used for seismic retrofitting of existing high–rise building, Jpn. Archit. Rev. 2 (2019) 269–286, https://doi.org/10.1002/2475-8876.12100.
[9] A.S. Pall, C. Marsh, Response of friction damped braced frames, J. Struct. Div.–ASCE 108 (1982) 1313–1323, https://doi.org/10.1061/JSDEAG.000596.
[10] R.C. Lin, Z. Liang, T.T. Soong, R.H. Zhang, P. Mahmoodi, An experimental study on seismic behaviour of viscoelastically damped structures, Eng. Struct. 13 (1991) 75–84, https://doi.org/10.1016/0141-0296(91)90011-Z.
[11] M.D. Symans, M.C. Constantinou, Passive fluid viscous damping systems for seismic energy dissipation, ISET J. Earthq. Technol 35 (1998) 185–206.
[12] I. Gidaris, A.A. Taflanidis, Performance assessment and optimization of fluid viscous dampers through life-cycle cost criteria and comparison to alternative design approaches, Bull. Earthq. Eng 13 (2015) 1003–1028, https://doi.org/10.1007/s10518-014-9646-5.
[13] Z. Lu, X. Chen, D. Zhang, K. Dai, Experimental and analytical study on the performance of particle tuned mass dampers under seismic excitation, Earthq. Eng. Struct. Dyn. 46 (2017) 697–714, https://doi.org/10.1002/eqe.2826.
[14] M.C. Constantinou, P. Tsopelas, W. Hammel, et al., Toggle-brace-damper seismic energy dissipation systems, J. Struct. Eng. 127 (2001) 105–112, https://doi.org/10.1061/(ASCE)0733-9445(2001)127:2(105).
[15] Y. Ribakov, A.M. Reinhorn, Design of amplified structural damping using optimal considerations, J. Struct. Eng. 131 (2005) 979–983, https://doi.org/10.1061/(ASCE)0733-9445(2003)129:10(1422).
[16] S. Berton, J.E. Bolander, Amplification system for supplemental damping devices in seismic applications, J. Struct. Eng. 131 (2005) 979–983, https://doi.org/10.1061/(ASCE)0733-9445(2005)131:6(979).
[17] E. Aydin, B. Öztürk, M. Dutkiewicz, Analysis of efficiency of passive dampers in multistorey buildings, J. Sound. Vib. 439 (2019) 17–28, https://doi.org/10.1016/j.jsv.2018.09.031.
[18] J.S. Hwang, J. Kim, Y.M. Kim, Rotational inertia dampers with toggle bracing for vibration control of a building structure, Eng. Struct. 29 (2007) 1201–1208, https://doi.org/10.1016/j.engstruct.2006.08.005.
[19] K. Ikago, K. Saito, N. Inoue, Seismic control of single-degree-of-freedom structure using tuned viscous mass damper, Earthq. Eng. Struct. Dyn. 41 (2012) 453–474, https://doi.org/10.1002/eqe.1138.
[20] M.C. Smith, Synthesis of mechanical networks: the inerter, IEEE Trans. Autom. Control. 47 (2002) 1648–1662, https://doi.org/10.1109/TAC.2002.803532.
[21] F.C. Wang, M.F. Hong, T.C. Lin, Designing and testing a hydraulic inerter, Proceedings of the Institution of Mechanical Engineers, Part C, J. Mech. Eng. Sci. 225 (2011) 66–72, https://doi.org/10.1243/09544062jmes2199.
[22] S.J. Swift, M.C. Smith, A.R. Glover, C. Papageorgiou, B. Gartner, Design and modelling of a fluid inerter, Int. J. Control. 86 (2013) 2035–2051, https://doi.org/10.1080/00207179.2013.842263.
[23] J. Yu, X. Dong, X. Su, X. Tao, X. Li, Design and testing of a semi-active inerter with magneto-rheological fluid valve, Smart Mater. Struct. 30 (2021) 105035, https://doi.org/10.1088/1361-665X/ac1ead.
[24] K. Saito, S. Kurita, N. Inoue, Optimum response control of 1-DOF system using linear viscous damper with inertial mass and its Kelvin-type modeling, J. Struct. Eng. 53 (2007) 53.
[25] I.F. Lazar, S.A. Neild, D.J. Wagg, Using an inerter-based device for structural vibration suppression, Earthq. Eng. Struct. Dyn. 43 (2014) 1129–1147, https://doi.org/10.1002/eqe.2390.
[26] L. Marian, A. Giaralis, Optimal design of a novel tuned mass-damper–inerter (TMDI) passive vibration control configuration for stochastically support-excited structural systems, Probab. Eng. Mech. 38 (2014) 156–164, https://doi.org/10.1016/j.probengmech.2014.03.007.
[27] Y. Nakamura, A. Fukukita, I.Yamazaki K.Tamura, T. Matsuoka, K. Hiramoto, K. Sunakoda, Seismic response control using electromagnetic inertial mass dampers, Earthq. Eng. Struct. Dyn. 43 (2014) 507–527, https://doi.org/10.1002/eqe.2355.
[28] W.G. Molyneux, Supports for Vibration Isolation, Her Majesty's Stationery Office, 1957. London.
[29] D.L. Platus, Negative-stiffness-mechanism vibration isolation systems. Vibration Control in microelectronics, optics, and Metrology 3786, International Society for Optics and Photonics, 1999, pp. 44–55. Available at: https://wp.optics.arizona.edu/optomech/wp-content/uploads/sites/53/2016/10/Platus-1992.pdf.
[30] A. Carrella, M.J. Brennan, T.P. Waters, Static analysis of a passive vibration isolator with quasi-zero-stiffness characteristic, J. Sound. Vib. 301 (2007) 678–689, https://doi.org/10.1016/j.jsv.2006.10.011.
[31] C.M. Lee, V.N. Goverdovskiy, A.I. Temnikov, Design of springs with "negative" stiffness to improve vehicle driver vibration isolation, J. Sound. Vib. 302 (2007) 865–874, https://doi.org/10.1016/j.jsv.2006.12.024.
[32] I. Kovacic, M.J. Brennan, T.P. Waters, A study of a nonlinear vibration isolator with a quasi-zero stiffness characteristic, J. Sound. Vib. 315 (2008) 700–711, https://doi.org/10.1016/j.jsv.2007.12.019.
[33] X. Shi, S. Zhu, Magnetic negative stiffness dampers, Smart Mater. Struct. 24 (2015) 072002, https://doi.org/10.1088/0964-1726/24/7/072002.
[34] Y. Shan, W. Wu, X. Chen, Design of a Miniaturized Pneumatic Vibration Isolator With High-Static-Low-Dynamic Stiffness, J. Vib. Acoust. 137 (2015) 045001. http://doi.org/10.1115/1.4029898.
[35] W Wu, X Chen, Y. Shan, Analysis and experiment of a vibration isolator using a novel magnetic spring with negative stiffness, J. Sound. Vib. 333 (2014) 2958–2970. http://doi.org/10.1016/j.jsv.2014.02.009.
[36] L. Chen, L. Sun, S. Nagarajaiah, Cable with discrete negative stiffness device and viscous damper: passive realization and general characteristics, Smart Struct. Syst. 15 (2015) 627–643. http://doi.org/10.12989/sss.2015.15.3.627.
[37] M. Wang, F. Sun, J. Yang, S. Nagarajaiah, Seismic protection of SDOF systems with a negative stiffness amplifying damper, Eng. Struct. 190 (2019) 128–141. http://doi.org/10.1016/j.engstruct.2019.03.110.
[38] S. Nagarajaiah, D. Sen, Apparent-weakening by adaptive passive stiffness shaping along the height of multistory building using negative stiffness devices and dampers for seismic protection, Eng. Struct. 220 (2020) 110754, https://doi.org/10.1016/j.engstruct.2020.110754.
[39] H. Luo, H. Zhu, K. Ikago, Optimal design of negative-stiffness dampers for improved efficiency of structural seismic isolation, J. Build. Eng. 68 (2023) 106172. http://doi.org/10.1016/j.jobe.2023.106172.
[40] F. Weber, C. Boston, M. Maślanka, An adaptive tuned mass damper based on the emulation of positive and negative stiffness with an MR damper, Smart Mater. Struct. 20 (2010) 015012. http://doi.org/10.1088/0964-1726/20/1/015012.
[41] Z. Zhao, Q. Chen, R. Zhang, Y. Jiang, C. Pan, A negative stiffness inerter system (NSIS) for earthquake protection purposes, Smart Struct. Syst. 26 (2020) 481–493. http://doi.org/10.12989/sss.2020.26.4.481.
[42] K. Ye, P. Nyangi, H∞ Optimization of Tuned Inerter Damper with Negative Stiffness Device Subjected to Support Excitation, Shock. Vib. 2020 (2020) 1–13. http://doi.org/10.1155/2020/7608078.
[43] E. Barredo, G.L. Rojas, J. Mayén, et al., Innovative negative-stiffness inerter-based mechanical networks, Int. J. Mech. Sci. 205 (2021) 106597. http://doi.org/10.1016/j.ijmecsci.2021.106597.
[44] H. Wang, H. Gao, J. Li, Z. Wang, Y. Ni, R. Liang, Optimum design and performance evaluation of the tuned inerter-negative-stiffness damper for seismic protection of single-degree-of-freedom structures, Int. J. Mech. Sci. 212 (2021) 106805. http://doi.org/10.1016/j.ijmecsci.2021.106805.
[45] K. Saito, Y. Sugimura, S. Nakaminami, H. Kida, N. Inoue, Vibration tests of 1-story response control system using inertial mass and optimized soft spring and viscous element, J. Struct. Eng. 54 (2008) 623–634.
[46] K. Ikago, Y. Sugimura, K. Saito, N. Inoue, Modal response characteristics of a multiple-degree-of-freedom structure incorporated with tuned viscous mass dampers, J. Asian. Archit. Build. Eng. 11 (2012) 375–382, https://doi.org/10.3130/jaabe.11.375.
[47] R. Jia, X. Ji, Y. Cheng, K. Ikago, Seismic response control of core wall structures using tuned viscous mass damper (TVMD) outriggers, Eng. Struct. 292 (2023) 116546. http://doi.org/10.1016/j.engstruct.2023.116546.
[48] N.U. Islam, R.S. Jangid, Optimum parameters of tuned inerter damper for damped structures, J. Sound. Vib. 537 (2022) 117218, https://doi.org/10.1016/j.jsv.2022.117218.

[49] L. Marian, The tuned mass damper inerter for passive vibration control and energy harvesting in dynamically excited structural systems, Diss. City University London (2015).
[50] L. Marian, A. Giaralis, Optimal design of inerter devices combined with TMDs for vibration control of buildings exposed to stochastic seismic excitation, in: Safety, Reliability, Risk and Life-Cycle Performance of Structures and Infrastructures-Proceedings of the 11th International Conference on Structural Safety and Reliability, CRC Press, 2013.
[51] H. Sun, L. Zuo, X. Wang, J. Peng, W. Wang, Exact H_2 optimal solutions to inerter-based isolation systems for building structures, Struct. Control. Health Monit. 26 (2019) e2357. http://doi.org/10.1002/stc.2357.
[52] H. Chen, P. Tan, Optimal design of TVMD with linear and nonlinear viscous damping subjected to white-noise excitation, Struct. Control. Health Monit. 28 (2021) e2694. http://doi.org/10.1002/stc.2694.
[53] R.S. Jangid, Optimum parameters and performance of tuned mass damper-inerter for base-isolated structures, Smart Struct. Syst. 29 (2022) 549–560. http://doi.org/10.12989/sss.2022.29.4.549.
[54] S. Djerouni, M. Abdeddaim, S. Elias, R. Rupakhety, Optimum Double Mass Tuned Damper Inerter for Control of Structure Subjected to ground motions, J. Build. Eng. 44 (2021) 103259. http://doi.org/10.1016/j.jobe.2021.103259.
[55] N.U. Islam, R.S. Jangid, Optimum parameters and performance of negative stiffness and inerter based dampers for base-isolated structures, Bull. Earthq. Eng 21 (2023) 1411–1438. http://doi.org/10.1007/s10518-022-01372-5.
[56] H. Li, K. Bi, H. Hao, Development of a novel tuned negative stiffness inerter damper for seismic induced structural vibration control, J. Build. Eng. 70 (2023) 106341. http://doi.org/10.1016/j.jobe.2023.106341.
[57] N.U. Islam, R.S. Jangid, Closed form expressions for H2 optimal control of negative stiffness and inerter-based dampers for damped structures, Struct 50 (2023) 7791–7809, https://doi.org/10.1016/j.istruc.2023.02.065.
[58] N.U. Islam, R.S. Jangid, Negative stiffness and inerter-based dampers: Novel seismic response control approach for base isolated liquid storage tanks, Struct 60 (2021) 1105860, https://doi.org/10.1016/j.istruc.2024.105860.
[59] S. Chowdhury, A. Banerjee, S. Adhikari, The optimal design of negative stiffness inerter passive dampers for structures, Int. J. Mech. Sci. 258 (2023) 108551, https://doi.org/10.1016/j.ijmecsci.2023.108551.
[60] Y.J. Tai, H.D. Wang, Z.Q. Chen, Vibration isolation performance and optimization design of a tuned inerter negative stiffness damper, Int. J. Mech. Sci. 241 (2023) 107948, https://doi.org/10.1016/j.ijmecsci.2022.107948.
[61] J. Wang, Y. Zhang, D.T.W. Looi, Analytical H∞ and H2 optimization for negative-stiffness inerter-based systems, Int. J. Mech. Sci. 249 (2023) 108261, https://doi.org/10.1016/j.ijmecsci.2023.108261.
[62] N. Su, J. Bian, S. Peng, Z. Chen, Y. Xia, Analytical optimal design of inerter-based vibration absorbers with negative stiffness balancing static amplification and dynamic reduction effects, Mech. Sys. Signal Proc. 192 (2023) 110235, https://doi.org/10.1016/j.ymssp.2023.110235.
[63] H. Gao, C. Xing, H. Wang, J. Li, Y. Zhang, Performance improvement and demand-oriented optimum design of the tuned negative stiffness inerter damper for base-isolated structures, J. Build. Eng. 63 (2023) 105488, https://doi.org/10.1016/j.jobe.2022.105488.
[64] K.K. Kiran, E. Noroozinejad Farsangi, V. Gharehbaghi, An innovative negative stiffness-inerter hybrid control device toward seismic-resilient structures, Innov. Infrastruct. Solut. 7 (2022) 310. http://doi.org/10.1007/s41062-022-00904-x.
[65] FEMA-356, Prestandard and commentary for the seismic rehabilitation of buildings, Fedral Emergency Management Agency, Washington, DC, 2000.
[66] FEMA-368, NEHRP recommended provisions for seismic regulations for new buildings and other structures, Building Seismic Safety Council, Washington, DC, 2001.
[67] JGJ297-2013, Technical specification for seismic energy dissipation of buildings, Ministry of Housing and Urban-Rural Development of China, Beijing, 2013 in Chinese.
[68] AIJ, Recommended Provisions for Seismic Damping Systems applied to Steel Structures, Architectural Institute of Japan, Tokyo, 2014 in Japanese.
[69] R. Zhang, Z. Zhao, C. Pan, K. Ikago, S. Xue, Damping enhancement principle of inerter system, Struct. Control. Hlth. 27 (2020) e2523. http://doi.org/10.1002/stc.2523.
[70] C. Pan, J. Jiang, R. Zhang, Y. Xia, Closed-form design formulae for seismically isolated structure with a damping enhanced inerter system, Struct. Control. Hlth. 28 (2021) e2840, https://doi.org/10.1002/stc.2840.
[71] L. Hao, H. He, P. Tan, K. Jin, X. Liu, Performance and efficiency oriented optimal design of tuned inerter damper for seismic response control of building structures, Int. J. Mech. Sci. 253 (2023) 108394. http://doi.org/10.1016/j.ijmecsci.2023.108394.
[72] Y. Li, P. Tan, S. Li, H. He, A novel tuned inerter eddy current damper: modeling, optimization, and evaluation, Eng. Struct. 285 (2023) 116026. http://doi.org/10.1016/j.engstruct.2023.116026.
[73] S.H. Crandall, W.D. Mark, Random vibration in mechanical systems, Academic Press, New York and London, 2014.
[74] H. He, C. You, P. Tan, Y. Xiang, Y. Yang, Effective damping ratio enhancement effect of tuned inerter dampers for seismic response control of civil structures, Eng. Struct. 279 (2023) 115504. http://doi.org/10.1016/j.engstruct.2022.115504.
[75] C. Pan, R. Zhang, Design of structure with inerter system based on stochastic response mitigation ratio, Struct. Control. Hlth. 25 (2018) e2169, https://doi.org/10.1002/stc.2169.
[76] FEMA-440, Improvement of nonlinear static seismic analysis procedures, Department of Homeland Security, Washington, DC, 2005.
[77] N. Kurata, T. Kobori, M. Takahashi, N. Niwa, H. Midorikawa, Actual seismic response controlled building with semi-active damper system, Earthq. Eng. Struct. Dyn. 28 (1999) 1427–1447, https://doi.org/10.1002/(SICI)1096-9845(199911)28:11<1427::AID-EQE876>3.0.CO;2-%23.
[78] J.P. Lynch, K.H. Law, Market-based control of linear structural systems, Earthq. Eng. Struct. Dyn. 31 (2002) 1855–1877, https://doi.org/10.1002/eqe.193.